Case Studies in Construction Materials 23 (2025) e05217

Contents lists available at ScienceDirect

Case Studies in Construction Materials

journal homepage: www.elsevier.com/locate/cscm

Hydration kinetics and modified model for effective water to cement ratio control in recycled aggregate concrete

Zhenhua Duan [a,b,*], Julun Li [a], Shuai Zou [c,**], Tianyong Huang [d,**], Bo Li [e], Zhangli Hu [f,**], Long Li [a]

[a] Department of Structural Engineering, College of Civil Engineering, Tongji University, Shanghai 200092, China
[b] Shanghai Key Laboratory of Urban Renewal and Spatial Optimization Technology, Shanghai 200092, China
[c] Department of Civil and Environmental Engineering, The Hong Kong Polytechnic University, Hong Kong, China
[d] Beijing Building Materials Academy of Science Research, Beijing 100041, China
[e] Department of Civil Engineering, University of Nottingham Ningbo China, Ningbo 315100, China
[f] School of Materials Science and Engineering, Southeast University, Nanjing 211189, China

ARTICLE INFO

Keywords:
Recycled aggregate concrete
Resource sustainability
Effective water to cement ratio
Moisture degree control
Hydration kinetics
Hydration model

ABSTRACT

The rapid urbanization surge has intensified the dual challenges of natural aggregate depletion and construction waste accumulation, necessitating sustainable solutions like recycled aggregate concrete (RAC). However, the higher water absorption of recycled aggregate (RA) disrupts the effective water-to-cement (w/c) ratio, critically impacting RAC performance. While prior research focused on RA water absorption ratio or empirical w/c ratio correlations of RAC, the interplay between RA moisture dynamics and hydration kinetics remained unexplored. This study bridges this gap by systematically investigating how RA initial moisture degree (D_{im}) and additional water ratio (R_{aw}) influence hydration behavior through isothermal calorimetry. A modified Krstulovic-Dabic hydration kinetics model, incorporating D_{im} and R_{aw} dependent correction coefficients (p_i, q_i), was developed to elucidate hydration mechanisms. Key findings reveal that RA with $D_{im} \leq 0.5$ reduced cumulative hydration heat by up to 11.8 % due to water absorption, while $D_{im} \geq 0.75$ enhanced heat release by up to 14.3 % via internal curing. The duration of the interactions at phase boundaries process gradually shortened and even disappeared with the increase of R_{aw} under low D_{im} ($\leq$ 0.5). A critical D_{im} threshold of 0.65 balanced water transport equilibrium, aligning effective and nominal w/c ratios. By linking RA moisture states to hydration kinetics, this study provides a framework for optimizing RAC mix designs with controllable effective w/c ratio, advancing sustainable construction practices.

Abbreviations: RAC, Recycled aggregate concrete; RA, Recycled aggregate; RC, Reference concrete; W/c, Water -to-cement ratio; D_{im}, Initial moisture degree; R_{aw}, Additional water ratio; ITZ, Interfacial transition zone; SSD, Saturated surface-dry; AD, Air dry; ρ_{app}, apparent density; WA_{24h}, 24 h water absorption; NG process, Nucleation and crystal growth process; I process, Interactions at phase boundaries process; D process, Diffusion process; DoH, Degree of hydration; D, Days; H, Hours.

* Corresponding author at: Department of Structural Engineering, College of Civil Engineering, Tongji University, Shanghai 200092, China.
** Corresponding authors.
E-mail addresses: zhduan@tongji.edu.cn (Z. Duan), frank-s.zou@connect.polyu.hk (S. Zou), hatty555@163.com (T. Huang), zhanglihu@seu.edu.cn (Z. Hu).

https://doi.org/10.1016/j.cscm.2025.e05217
Received 1 June 2025; Received in revised form 12 August 2025; Accepted 23 August 2025
Available online 25 August 2025

1. Introduction

Since the onset of the 21st century, China has witnessed a surge in its urbanization rate, soaring from 38 % to 61 %[1]. This rapid urban expansion has led to the substantial extraction and depletion of natural sand and gravel resources[2,3]. On the one hand, environmental degradation, natural aggregates shortage, and rising prices have escalated as pressing concerns. On the other hand, solid wastes resulting from the demolition of old buildings has emerged as the primary contributor to municipal waste, significantly endangering the ecological environment[4–6]. Recycled aggregate concrete (RAC), which uses recycled aggregates (RA) from buildings demolition[7–10], offers a promising solution to the above-mentioned dual challenges and is garnering increasing research interests[11,12].

Although RAC have been applied in some exemplary roads and buildings[13,14], its adoption in mainstream engineering projects remains marginal[15]. The main reason is that the old mortar attached to the surface of RA greatly increases the porosity and water absorption[16,17]. It is reported that the water absorption of recycled coarse aggregate is 3.4–11.3 times higher than that of natural coarse aggregate[16,18,19]. The water absorption of recycled fine aggregate is 2.1–8.5 times higher than that of natural fine aggregate [20,21]. Therefore, many scholars have noticed the significant influence of compensating water on the performance of RAC and proposed two main strategies of compensating water. The one method involved pre-wetting RAs to a moisture content to meet the demand of absorbing water partially[22–25]. The main disadvantage of this approach is that it can't achieve uniform regulation of the moisture content of large-scale RA particles[26,27]. The other method is to add extra moisture during the preparation of RAC[28]. However, there is no consensus on the amount of exact water to be compensated. In fact, the shortcomings of these two methods lead to the true amount of water absorbed by RA in fresh concrete system cannot be accurately measured.

The drawbacks of the two aforementioned countermeasures may result in significant fluctuations in the workability of RAC [29–32]. The application of RA with lower moisture content leads to the smaller initial slump of concrete. This is because RA absorbs water from cement slurry during mixing, resulting in loss of free water. Research findings indicate that the water absorption kinetics of RA are fastest in the first few minutes of contact with water[33], and the slump loss of RAC is also the largest during this period. Pre-wetting treatment of RA is helpful to improve the workability of RAC. Under a fixed total water supply, the larger the initial moisture state of RA, the more moisture RA pre-absorbed, indicating that less mixing water is added in the mixing process of RAC. This will also cause the workability loss of fresh concrete.

Numerous studies have confirmed the significant impact of the aforementioned two moisture regulation measures on the mechanical properties of RAC[34–36], but the conclusions vary considerably. Most of the research findings indicate that partially saturated RAs absorb a small amount of water from the slurry, which results in a slight decrease in the w/c ratio of concrete[37], thereby increasing the compressive strength. However, the optimal moisture content of RA has not been quantitatively studied[25]. Other reports show that the RA with lower moisture content can improve the compressive strength of concrete under the same total water consumption[12,38]. This is because the unre-wetted RAs absorb more water from the paste and cement particles are adsorbed in the surface pores of RAs. This enhances the bond strength between RA and cement slurry and improves the interfacial transition zone (ITZ) compactness[39–41]. This mechanism is named as the "nail effect"[24,42]. RA in a saturated surface-dry (SSD) state has the greatest negative impact on the compressive strength. This SSD RA increases the effective w/c ratio of the ITZ via releasing moisture into the cement slurry and impair the performance of the ITZ[43–45]. However, some scholars believe that pre-wetted RA enhances the elastic modulus of the ITZ between the old and new cement paste, but has a negative impact on the elastic modulus of the ITZ between the aggregate and the new cement paste[46–48].

Consequently, elucidating the moisture transfer mechanism between RA and slurry and proposing an accurate method to determine the effective w/c ratio are conducive to control and predict the performance of RAC accurately[49], which is of great significance to the application and promotion of the RA in actual engineering projects[50,51]. Li et al.[52] isolated RA from slurry within 5 h, then dried the slurry at 1050°C to ascertain water content. The study uncovered the time-dependent water absorption of dried RA, linking w/c ratio to RA water absorption. However, sampling limitations may impact result accuracy due to the incomplete RA-slurry separation. Comparatively, Ge et al.[53] further investigated the effective water absorption of RA in different w/c ratios paste and proposed a calculation model for the compressive strength of RAC. Dang et al.[54] studied the impact of additional water on hydration heat of RAC using calorimetry and proved that adding water delayed hydration and affected hydration's peak appearance and height. The elevated effective w/c ratio by additional water was identified as the primary cause. Maimouni et al.[55] evaluated the water absorption of RA via RAC's workability index by assuming a direct correlation between workability and effective w/c ratio. Adessina et al.[56] studied the mechanical and durability properties of RAC with the same assumption. However, the RA in SSD condition may release water into the slurry, resulting in an increase of effective w/c ratio.

As mentioned above, previous studies have focused on quantifying RA water absorption or correlating w/c ratios with RAC properties but lacked insights into how RA moisture dynamics influence hydration kinetics[57]. While the water absorption behavior of RA is a physical process, it fundamentally modifies the chemical interactions between cementitious materials and water, consequently influencing multiple properties of RAC[58–60]. Therefore, clarifying the water transport mechanism between RA and paste and proposing a method to determine the effective w/c ratio based on hydration kinetics is of great significance. This study explored how the initial moisture degree (D_{im}) of RA and additional water ratio (R_{aw}) affect the hydration characteristics and degree of RAC through hydration heat analysis. We constructed a modified Krstulovic-Dabic hydration kinetic model to capture the dynamic process of RA water absorption and release, which enables a detailed study of the hydration mechanism. The results are expected to provide an approach for optimizing RAC mix designs to have a controllable effective w/c ratio, thereby improving the predictability of RAC performance and promoting sustainable construction practices.

2. Experimental program

2.1. Materials

The cement utilized in this study is the standard P·I 42.5 cement manufactured by Shandong Lucheng Cement Co., Ltd., with its chemical composition shown in Table 1. ISO standard sand and RA sourced from Youhong Waste Resource Treatment Company, Shanghai were employed as aggregates. In order to reduce the impact of the difference in particle gradation between RA and ISO standard sand, the RA was washed, dried, sieved, and mixed by referring to GB/T 14684–2022[61] to attain similar particle gradation with the ISO standard sand, as shown in Fig. 1. The comparison of apparent density (ρ_{app}) and 24 h water absorption ($WA_{24\,h}$) between RA and ISO standard sand is shown in Table 2.

2.2. Experiments and testing methods

2.2.1. Initial moisture degree and additional water ratio

In this study, the initial water degree (D_{im}) is defined as the ratios of the initial aggregate water content to its total water absorption content. The preparation methods of the RAs with different D_{im} values are shown in Fig. 2 and described as follows: (i) Drying the RA in an oven at 105℃ to absolute-dry state; (ii) Evenly spraying water onto the RA while continuously mixing it to ensure uniform absorption. The mass of RA was monitored in real-time to ensure that the sprayed water was fully absorbed by the RA. As shown in Fig. 3, the value of D_{im} was controlled as 0, 0.25, 0.5, 0.75 and 1.0 and the target RA was sealed and stored for later use. The saturated surface-dry condition of RA was designed by referring to GB/T 14684–2022[61]. Except for the D_{im} value, additional water ratio R_{aw} was determined according to $D_{im} + R_{aw}$. For example, the mix design of D_{im}= 0.5 and $D_{im} + R_{aw} = 0.6$ means that the initial moisture degree of the RCA is the 50 % of its total water absorption content and another 10 % of its total water absorption content was provided as additional water. In this study, the maximum $D_{im} + R_{aw}$ value of RA was design as 1.0 to not higher than its water content under saturated surface dry state.

2.2.2. Formulation design

The mix proportions of RAC are shown in Table 3, which are named as RAC $D_{im} + R_{aw}$. Five groups of RAC samples developed by RA of 0–1.0 D_{im} and R_{aw}= 0 were designed for investigating the effect of D_{im}. Meanwhile, RA of same D_{im} while different R_{aw} were prepared to analyze the effect of R_{aw}. It should be noticed that the mass of RA in Table 3 is essentially the total mass of RAs and the water contained in RAs. Therefore, the difference in mass of RAs is caused by the difference in mass of moisture contained in RAs. In other words, the volume and mass of RAs remain fixed, and the mass of water contained in RAs changes.

Reference concrete (RC) groups prepared with ISO standard sand under w/c ratio ranging from 0.36 to 0.64 were listed in Table 4. The RC and RAC 0 + 0 groups attain same mix proportion except for different aggregate usage. The mass of the standard sand is calculated by the equivalent volume substitution method based on the RA amount in RAC test group.

2.2.3. Samples preparation

The hydration testing samples (volume approximately 50 ml) were prepared according to the above-mentioned mix proportions as follows[62]:

(1) Pouring and evenly mixing the fine aggregates and cement in the testing cup.
(2) Injecting deionized water and continuously stirring for 1 min.
(3) Sealing and quickly placing the prepared samples into the testing chamber for minimizing heat loss.

2.2.4. Hydration heat

The hydration heat evolution rate and cumulative hydration heat of the prepared samples were tested by the TAM Air 8-channel isothermal calorimeter produced by TA Instruments. The testing temperature was set as 25℃ with data acquisition frequency of 1 time/min and testing period of 168 h.

2.3. Hydration kinetics model

The Krstulovic-Dabic model serves as a pivotal tool for studying the hydration kinetics of cement-based materials[63,64], which categorizes the hydration process into three processes: nucleation and crystal growth (NG), interactions at phase boundaries (I), and diffusion (D). The related hydration equations are shown as below[63]:

(NG):

Table 1
Chemical composition of cement (%).

Composition	CaO	SiO_2	Al_2O_3	Fe_2O_3	MgO	SO_3	Other	L.O.I
Cement	62.09	21.47	5.34	3.47	3.20	2.63	1.30	0.50

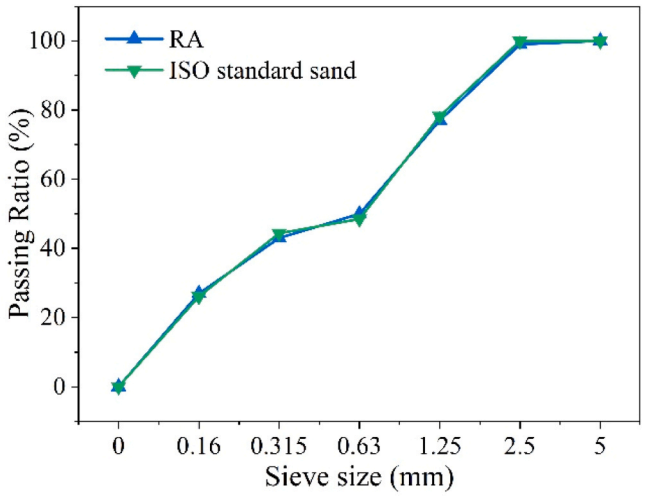

Fig. 1. Particle gradation of RA and ISO standard sand.

Table 2
ρ_{app} and $WA_{24\,h}$ comparison.

Type of aggregate	ρ_{app} (g/cm^3)	$WA_{24\,h}$ (%)
RA	2191.3	12.7
ISO standard sand	2657.6	0.9

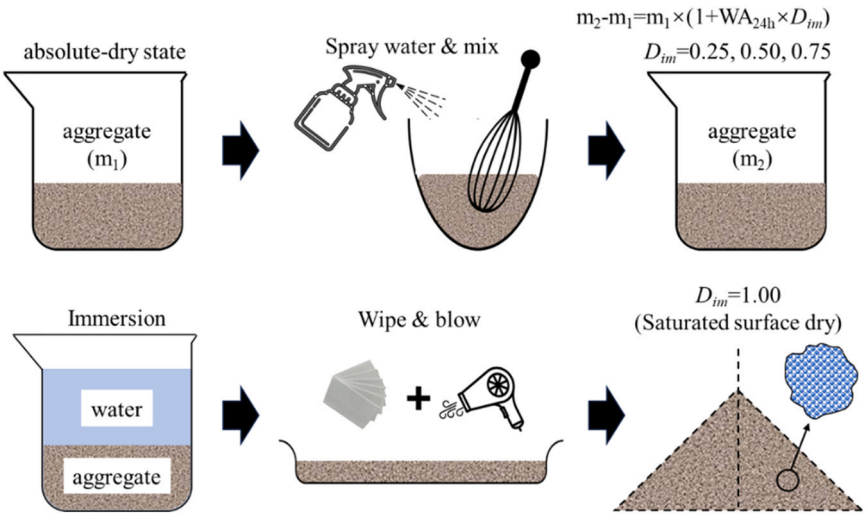

Fig. 2. Procedure for adjusting the D_{im} of RAs.

$$[-\ln(1-\alpha)]^{\frac{1}{n}} = K_1(t-t_0) = K_{NG}(t-t_0) \tag{1}$$

(I):

$$[1-(1-\alpha)^{\frac{1}{3}}]^1 = K_2 r^{-1}(t-t_0) = K_I(t-t_0) \tag{2}$$

(D):

$$[1-(1-\alpha)^{\frac{1}{3}}]^2 = K_3 r^{-2}(t-t_0) = K_D(t-t_0) \tag{3}$$

Where: α represents the hydration degree of cementitious materials; n is the geometric crystal growth index, also known as reaction

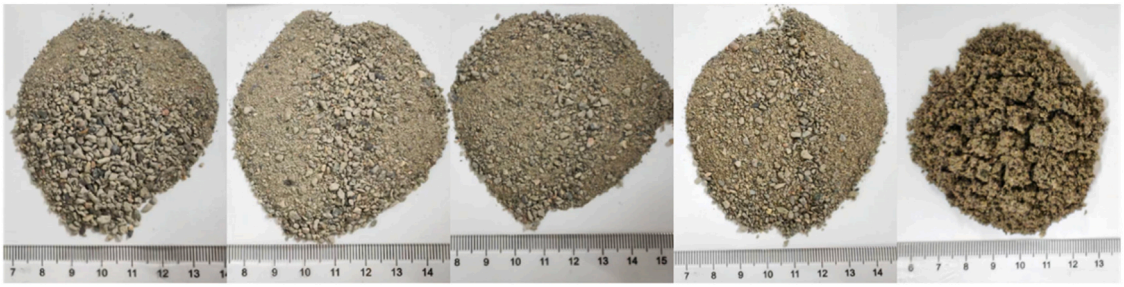

Fig. 3. RAs with different D_{im}.

Table 3
Mix proportions of RAC.

No.	Cement	RA	Water	W/C
RAC 0 + 0	25	36.0734	9.0909	0.363636
RAC 0 + 0.6			13.1600	0.5264
RAC 0 + 0.7			13.8382	0.553528
RAC 0 + 0.8			14.5163	0.580652
RAC 0 + 0.9			15.1945	0.60778
RAC 0 + 1.0			15.8727	0.634908
RAC 0.25 + 0	25	37.7688	9.0909	0.363636
RAC 0.25 + 0.35			11.4645	0.45858
RAC 0.25 + 0.45			12.1427	0.485708
RAC 0.25 + 0.55			12.8209	0.512836
RAC 0.25 + 0.65			13.4991	0.539964
RAC 0.25 + 0.75			14.1772	0.567088
RAC 0.5 + 0	25	39.4643	9.0909	0.363636
RAC 0.5 + 0.1			9.7691	0.390764
RAC 0.5 + 0.2			10.4473	0.417892
RAC 0.5 + 0.3			11.1254	0.445016
RAC 0.5 + 0.4			11.8036	0.472144
RAC 0.5 + 0.5			12.4818	0.499272
RAC 0.75 + 0	25	41.1597	9.0909	0.363636
RAC 0.75 + 0.05			9.4300	0.3772
RAC 0.75 + 0.15			10.1082	0.404328
RAC 0.75 + 0.25			10.7863	0.431452
RAC 1.0 + 0	25	42.8552	9.0909	0.363636

Table 4
Mix proportions of RC.

No.	Cement	Standard sand	Water	W/C
RC	25	43.7500	9.0909	0.363636
RC1			8.5	0.34
RC2			9.0	0.36
RC3			9.5	0.38
RC4			10.0	0.40
RC5			10.5	0.42
RC6			11.0	0.44
RC7			11.5	0.46
RC8			12.0	0.48
RC9			12.5	0.5
RC10			13.0	0.52
RC11			13.5	0.54
RC12			14.0	0.56
RC13			14.5	0.58
RC14			15.0	0.60
RC15			15.5	0.62
RC16			16.0	0.64

order; t represents the time of hydration reactions; t_0 is the end time of induction period; r represents the radius of reacting particles; K_1, K_2, K_3 represent the reaction rate constant; K_{NG}, K_I, K_D represent apparent reaction rate constant.

In order to convert the tested hydration heat data into parameters required for kinetic analysis, the Knudson extrapolation equation is applied in the Krstulovic-Dabic model, as shown in Eq. 4[65,66].

$$\frac{1}{Q(t)} = \frac{1}{Q_{\max}} + \frac{t_{50}}{Q_{\max}(t-t_0)} = \frac{1}{Q_{\max}}\left(1 + \frac{t_{50}}{t-t_0}\right) \tag{4}$$

Where: $Q(t)$ represents the hydration heat of cementitious materials at time t; Q_{max} represents the total hydration heat of cementitious material until end of hydration; t_{50} represents the hydration time required for releasing 50 % Q_{max}, also knowing as half-life; (t-t_0) represents the hydration time calculated from the end of induction time (i.e., the start of the acceleration period). Accordingly, Q_{max} and t_{50} can be calculated based on Eq. 4. After that, the degree of hydration $\alpha(t)$ and the actual hydration rate $d\alpha/dt$ can be obtained by substituting Q_{max} and t_{50} into Eqs. 5 and 6:

$$\alpha(t) = \frac{Q(t)}{Q_{\max}} \tag{5}$$

$$\frac{da}{dt} = \frac{dQ}{dt} \bullet \frac{1}{Q_{\max}} \tag{6}$$

Furthermore, the kinetic parameters n, K_{NG}, K_I, and K_D can be determined through linear fitting by substituting the degree of hydration α into Eqs. 7–9. Subsequently, the relationships between $F_{NG}(\alpha)$, $F_I(\alpha)$, $F_D(\alpha)$ and α can be attained by substituting the mentioned kinetic parameters into Eqs. 7–9. Where, the $F_{NG}(\alpha)$, $F_I(\alpha)$, $F_D(\alpha)$ represent the reaction mechanism function, characterizing the NG, I, and D processes. Finally, the hydration mechanism and degree of RAC can be analyzed by plotting the relationships between $F_{NG}(\alpha)$, $F_I(\alpha)$, $F_D(\alpha)$, $d\alpha/dt$, and α.

NG process differential form:

$$\left[\frac{da}{dt}\right]_{NG} = F_{NG}(\alpha) = K_{NG} n (1-\alpha)[-\ln(1-\alpha)]^{\frac{n-1}{n}} \tag{7}$$

I process differential form:

$$\left[\frac{da}{dt}\right]_{I} = F_I(\alpha) = K_I \bullet 3(1-\alpha)^{\frac{2}{3}} \tag{8}$$

D process differential form:

$$\left[\frac{da}{dt}\right]_{D} = F_D(\alpha) = K_D \bullet \frac{3}{2} \bullet \frac{(1-\alpha)^{\frac{2}{3}}}{1-(1-\alpha)^{\frac{1}{3}}} \tag{9}$$

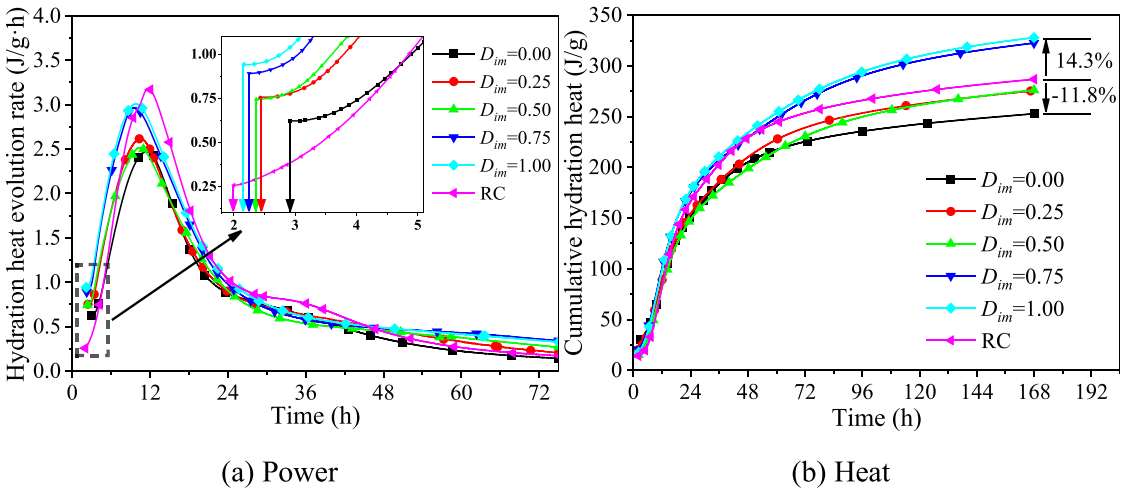

Fig. 4. Evolution rate and cumulative hydration heat of RAC with different D_{im}.

3. Results and discussion

3.1. Early hydration characteristics

3.1.1. Effect of initial moisture degree

Fig. 4 shows the heat evolution rate and cumulative hydration heat of RC and RAC under different RA D_{im} without R_{aw}. It can be observed from Fig. 4(a) that the heat evolution rate of RC sample reached a trough before beginning to rise after 2 h of hydration, which is generally regarded as the induction period of cement hydration. It is evident that the induction period progressively decreased with the rise of RA D_{im}. This occurs because RA with a lower D_{im} would diminish the available water content for hydration, thus resulting in a slower dissolution rate of cement particles and a prolonged induction period.

Regarding the acceleration period following the induction phase, it demonstrated a gradual reduction to 8.5, 8.13, 8.07, 7.7, and 7.4 h with RA D_{im} of 0.00, 0.25, 0.50, 0.75, and 1.00, respectively, however, all lowered than that of RC group. The dissolution theory proposed by Juilland can explain this phenomenon well[67–69]. Upon contact with water, the dissolution of cement particles and the moisture absorption of RA commence concurrently. RA with a higher D_{im} value absorb water more slowly. This implies that RA with a higher D_{im} value have a weaker effect on accelerating the increase in ionic concentration in the solution and reducing the degree of undersaturation. The shorter the induction period, the later the hydration reaction enters the acceleration period.

After 46.3 h of hydration, the heat evolution rate of RC gradually decreased below that of RAC groups with RA. Despite identical mixing water content across all groups, the RAC system contains more water than the RC system due to the internal water storage of RA. During the stable hydration period, the RA gradually released water into the paste, resulting in a slower decline in the heat release

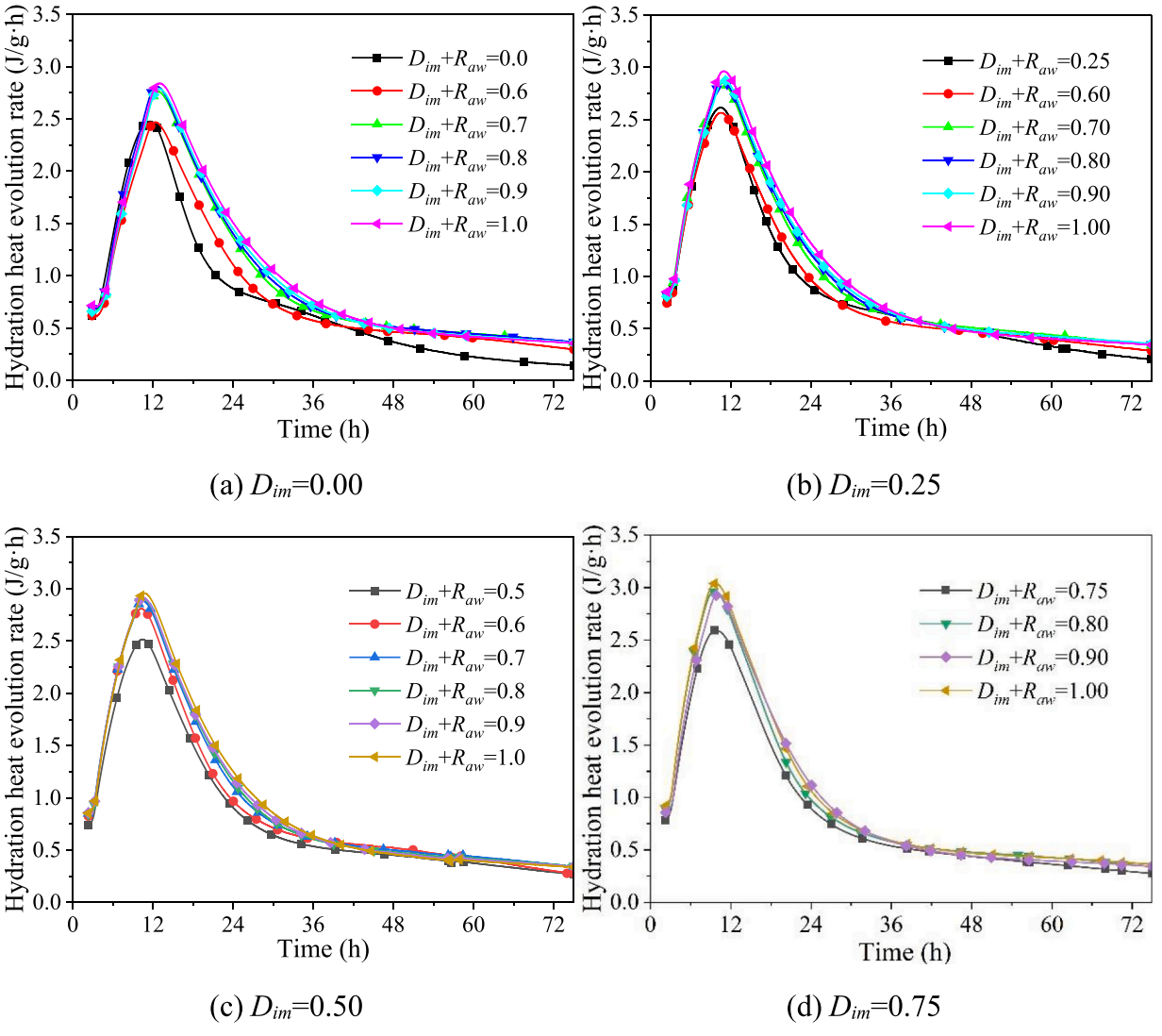

Fig. 5. Hydration heat evolution rate of RAC under different D_{im} and D_{im} + R_{aw}.

rate of RAC compared to RC. However, oven-dry RA does not introduce additional water into the RAC system. Therefore, the heat release rate of RAC prepared with oven-dry RA remained lower than that of RC during the stable hydration period.

As shown in Fig. 4(b), the 7-day cumulative hydration heat of RA D_{im}= 0 (oven dry) group was 11.8 % lower than that of RC group. However, for D_{im}= 1.0 (SSD) group, its 7-day cumulative hydration heat was 14.3 % higher than that of RC group. This phenomenon indicates that the initial water content of RA significantly affects the cumulative hydration heat of RAC. Typically, the water absorption capacity of RA decreased with the increase of D_{im}, which allowed more water to be accessible for hydration, leading to heightened levels of hydration in RAC.

Fig. 4(b) also indicates that the RC group with standard sand showed a higher 7d cumulative hydration heat than RA with D_{im} value of 0, 0.25, and 0.5, however, lower than that of groups with RA D_{im} value of 0.75 and 1.0. This phenomenon indicates that the water absorption behavior of RA with a lower D_{im} value adversely affected the hydration in concrete. However, a higher initial water content of RA could effectively promote the hydration due to the internal curing effect of the moisture released by RA.

3.1.2. *Effect of additional water ratio*

Fig. 5 shows the effect of additional water on hydration heat evolution rate. When the D_{im} was fixed, the appearance time and duration of the induction period were found to be similar, and the different R_{aw} caused very limited changes on the heat release rate during the induction period. However, R_{aw} played a significantly effect on the acceleration and deceleration periods. The peak heat release rate increased with the R_{aw}. As the hydration progressed into the deceleration stage, increasing the amount of additional water can effectively slow down the decline of the heat release rate. Moreover, the mitigation effect became more pronounced with a lower R_{aw}. This is attributed to the increased water absorption capacity of RA at lower R_{aw} during the initial phases, leading to an improved

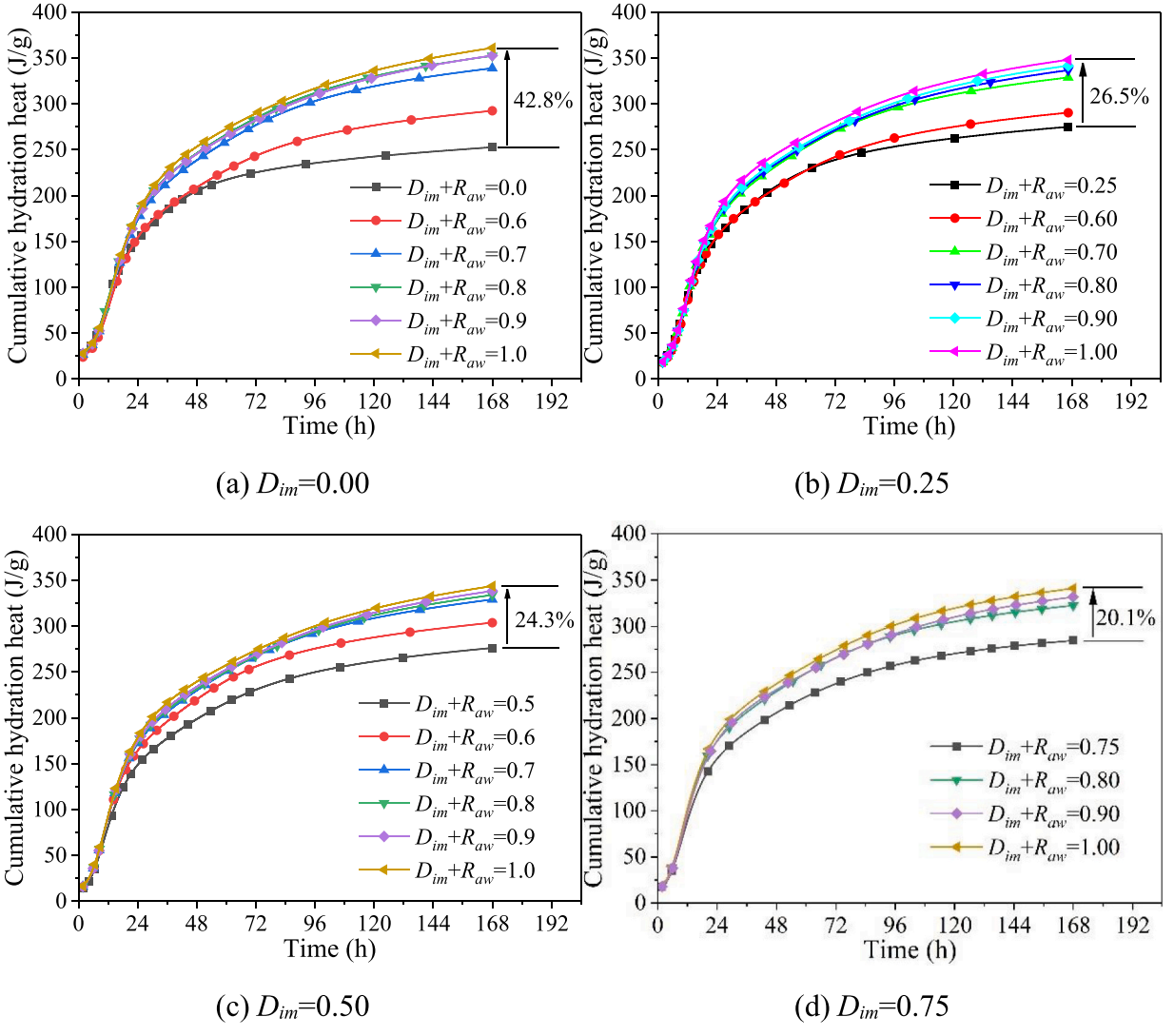

Fig. 6. Cumulative hydration heat of RAC under different D_{im} and D_{im} + R_{aw}.

internal curing effect during the later hydration stages.

As shown in Fig. 6, the 7d cumulative hydration heat of RAC was observed to rise with the increase of R_{aw}. This observation implies that the water absorption characteristics of RA exerted a somewhat adverse influence on RAC hydration, while additional mixing water can effectively promote hydration to alleviate this negative impact. However, this alleviating effect weakened as the increase of R_{aw}, eventually reaching a critical threshold. Specifically, when D_{im} value no more than 0.5, the inclusion of extra water can notably promote the hydration when $D_{im} + R_{aw}$ not exceeding 0.7. However, the efficacy of this promotion diminished with higher amounts of added water, specifically when $D_{im} + R_{aw}$ surpassed 0.7. This threshold can be extended to 0.8 when D_{im} was 0.75. In terms of the impact of R_{aw} on cumulative hydration heat increasing degree, the findings revealed that the higher the RA D_{im}, the lower the increasing degree, which corresponds to be 42.8 %, 26.5 %, 24.3 %, and 20.1 % for D_{im} of 0, 0.25, 0.5, and 0.75, respectively. This indicated that the cumulative hydration heat of RAC can be less affected by the additional water when using higher initial water content of RA.

3.2. Hydration kinetics parameters

3.2.1. Total heat release Q_{max} and half-life t_{50}

As indicated by Eq. 4, $\frac{1}{Q(t)}$ is linear related to $\frac{1}{t-t_0}$, enabling the determination of the total heat release Q_{max} and half-life t_{50} through the slope and intercept obtained via linear fitting. Therefore, the experimental data from the above hydration test was fitted by Krstulovic-Dabic model, as shown in Fig. 7 taken RAC0 + 0 as an example. The Q_{max} and t_{50} values of all RAC samples were obtained and listed in Table 5.

It can be observed that both maximum heat release Q_{max} and hydration half-life t_{50} of RAC increased with R_{aw} under the same D_{im}. This is consistent with the experimental results in Section 3.1.2. The larger the R_{aw}, the more free water absorbed by RA can be gradually released to slow down the decrease of hydration rate in the later stages, thus extending the half-life. Additionally, the Q_{max} of RAC was found to decrease with the increase of D_{im} when $D_{im} + R_{aw} = 1.0$. This is because Q_{max} depends mainly on the amount of water contained in the paste, so when the total water content within the RAC system is the same, the lower D_{im} value of recycled aggregate correspond to higher moisture content in the paste, leading to larger Q_{max} values.

3.2.2. Crystallization nucleation index and reaction rate constants

By performing linear fitting on the data obtained from isothermal calorimetry using Eqs. 1–3, the crystallization nucleation index n, and the reaction rate constants K_{NG}, K_I, and K_D can be obtained, which are the hydration kinetics parameters. Taking RAC0 + 0 as an example, the linear fitting results of the NG, I, and D reaction processes are shown in Fig. 8. Based on this method, the hydration kinetics parameters of all the RAC samples were fitted and listed in Table 6.

It can be found that the reaction rate constants K_{NG}, K_I, and K_D all decreased with the increase of R_{aw} with fixed D_{im}. When $D_{im} + R_{aw} = 1.0$, K_{NG} and K_I increased with the increase of D_{im}, along with a negligible minor fluctuation of K_D. The values of K_{NG} were about 7–16 times higher than the K_I, and about 29–39 times higher than K_D. This is because the hydration of cement during the NG process is autocatalytic and the hydrated products grow rapidly. The expansion of crystal nuclei prior to the interaction of hydration products amplifies the specific surface area of the hydration product phase, consequently fostering the early hydration reaction. However, the reaction rate of I process is affected by the ion concentration in the solution, the growth space of hydration products, and the specific surface area of crystals. The additional water not fully absorbed by RA would dilute the ionic concentration in the solution, subsequently impacting the pace of the RAC hydration process. As hydration time increases, the reaction transitions into phase diffusion process, markedly reducing the porosity and permeability of the paste. Additionally, the formation of a dense C-S-H layer over $Ca(OH)_2$ crystals and unhydrated cement particles significantly heightens the diffusion barrier against water, Ca^{2+}, and OH^- towards unreacted

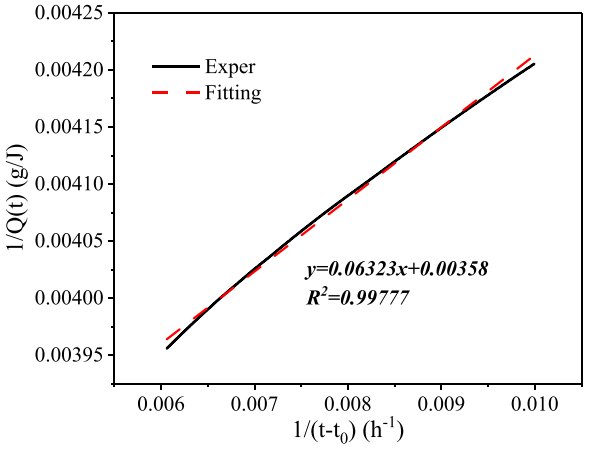

Fig. 7. Determination of Q_{max} and t_{50}.

Table 5
Total heat release (Q_{max}) and half-life (t_{50}) of RAC.

No.	*Q(7d)*	Q_{max}/(J/g)	t_{50}/(h)	Kundsen equation	R^2
RAC0 + 0	252.80	279.33	20.45	y = 0.06323x+ 0.00358	0.99777
RAC0 + 0.6	292.52	338.98	28.57	y = 0.07761x+ 0.00295	0.99988
RAC0 + 0.7	338.92	398.41	30.58	y = 0.07254x+ 0.00251	0.99994
RAC0 + 0.8	352.44	421.94	32.33	y = 0.07720x+ 0.00237	0.99994
RAC0 + 0.9	352.76	429.19	33.92	y = 0.08323x+ 0.00233	0.99997
RAC0 + 1.0	361.08	440.53	33.67	y = 0.08161x+ 0.00227	0.99999
RAC0.25 + 0	275.20	310.56	24.27	y = 0.06869x+ 0.00322	0.99821
RAC0.25 + 0.35	290.40	337.84	28.48	y = 0.07906x+ 0.00296	0.99957
RAC0.25 + 0.45	328.80	386.10	30.00	y = 0.07480x+ 0.00259	0.99978
RAC0.25 + 0.55	336.80	406.50	32.65	y = 0.08374x+ 0.00246	0.99985
RAC0.25 + 0.65	341.60	414.94	33.65	y = 0.08518x+ 0.00241	0.99986
RAC0.25 + 0.75	348.00	423.73	32.18	y = 0.08376x+ 0.00236	0.99986
RAC0.5 + 0	276.10	319.49	27.88	y = 0.08169x+ 0.00313	0.99987
RAC0.5 + 0.1	303.70	339.65	27.40	y = 0.07289x+ 0.00294	0.99969
RAC0.5 + 0.2	329.00	380.63	31.42	y = 0.08055x+ 0.00262	0.99992
RAC0.5 + 0.3	333.90	393.23	33.05	y = 0.08605x+ 0.00254	0.99996
RAC0.5 + 0.4	338.30	404.94	34.50	y = 0.09041x+ 0.00247	0.99998
RAC0.5 + 0.5	343.60	413.73	34.10	y = 0.09072x+ 0.00242	0.99999
RAC0.75 + 0	311.92	365.41	28.07	y = 0.07246x+ 0.00274	0.99991
RAC0.75 + 0.05	322.45	387.87	26.53	y = 0.07649x+ 0.00305	0.99951
RAC0.75 + 0.15	331.66	409.84	31.55	y = 0.08104x+ 0.00244	0.99985
RAC0.75 + 0.25	340.95	401.61	32.02	y = 0.08719x+ 0.00249	0.99980
RAC1.0 + 0	327.82	384.62	28.65	y = 0.07386x+ 0.00260	0.99983

cement particles in the RAC system, leading to a very low reaction rate for the D process.

The parameter *n* signifies the nucleation of crystallization and crystal growth of hydration products. Although this nucleation index fluctuated with D_{im} and R_{aw}, the variation remained within a narrow margin of ±5 %. However, the correlation researches show that the parameter n decreases with the increase of w/c, which attributed to the decrease of saturation of cement paste solution[70]. The main reason for the difference between the experimental results and the correlation researches is that the original Krstulovic-Dabic hydration kinetics model did not take into account the D_{im} of RA and R_{aw} as the influencing factors. Therefore, the hydration kinetics model has been modified in this paper. The modified method and the modified hydration dynamics model are shown in Section 3.3. The crystal nucleation index $p_{NG}n$ obtained by fitting the modified hydration dynamics model is shown in Table 6. The results show that the parameter $p_{NG}n$ decreases with the increase of w/c, and the decreasing rate gradually changes. This result is consistent with the previous research results[71] and also proves the reliability and superiority of the modified hydration kinetics model in analyzing the hydration dynamics of RAC.

3.3. Modification of hydration kinetics model

Although the Krstulovic-Dabic model is extensively employed in researching the mechanisms of cement hydration due to its exceptional practicality, the fitting efficacy of the model is unsatisfactory for RAC since the impact of the water absorption and release characteristics of RA on hydration is not considered. Taking RAC0 + 0 as an example, the fitting results from Krstulovic-Dabic model are shown in Fig. 9.

Thus, the model was modified in this study by introducing two correction coefficients, p_i and q_i, associated with D_{im} and R_{aw}, as depicted in Eqs. 10–12. The coefficient p_{NG} can be regarded as a correction for index *n*. The correlation analysis was conducted on correction coefficients p_i and q_i with calculation formulas proposed in Table 7. Due to the rapid and unstable hydration in NG process, p_{NG} shows a moderate level of correlation with D_{im} and R_{aw}. While p_I, p_D and q_{NG} show a strong correlation with D_{im} and R_{aw}. q_I and q_D are constants independent of D_{im} and R_{aw}. Comparing Fig. 9 with Fig. 10(a), the fitting effect of the modified hydration kinetic model on the RAC hydration rate curve was significantly improved.

NG process:

$$\left[\frac{da}{dt}\right]_{NG} = F_1(\alpha) = K_{NG}(p_{NG}n)(1-\alpha)[-\ln(1-\alpha)]^{\left(1-\frac{1}{p_{NG}\bullet n}\right)} - q_{NG} \tag{10}$$

I process:

$$\left[\frac{da}{dt}\right]_{I} = F_2(\alpha) = p_I \bullet K_I \bullet 3(1-\alpha)^{\frac{2}{3}} - q_I \tag{11}$$

D process:

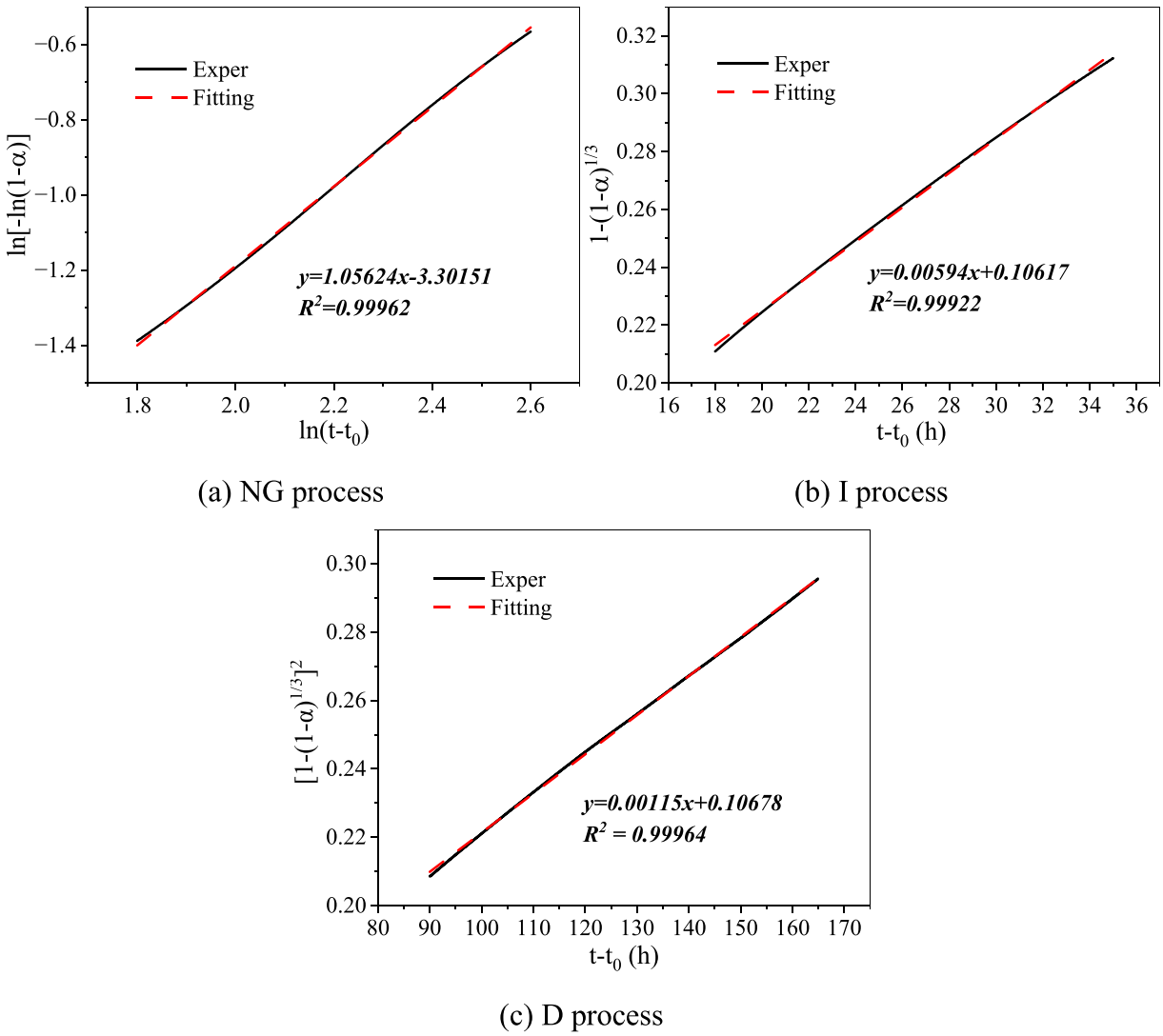

Fig. 8. Linear fitting for determining K_{NG}, K_I, and K_D.

$$\left[\frac{da}{dt}\right]_D = F_3(\alpha) = p_D \bullet K_D \bullet \frac{3}{2} \bullet \frac{(1-\alpha)^{\frac{2}{3}}}{1-(1-\alpha)^{\frac{1}{3}}} - q_D \tag{12}$$

3.4. Hydration kinetics of RAC based on modified model

Figs. 10–14 show the tested and simulated hydration rate curves of RAC with RA D_{im} of 0, 0.25, 0.5, 0.75, and 1.0. This study ignores the first exothermic peak mainly caused by the dissolution heat and only simulates the reaction process after the induction period, as shown in Table 8. The fitting results based on the modified model was listed in Table 8, where α_1 and α_2 represent the hydration degree of RAC at the transition from the NG process to the I process and from the I process to the D process, respectively.

As shown in Fig. 10, when D_{im}= 0 and $D_{im} + R_{aw} \leq$ 0.9, the hydration kinetics of RAC undergoes three processes: NG, I, and D. For the NG process, the higher the R_{aw}, the more difficult it is for C-S-H and $Ca(OH)_2$ in the paste to reach supersaturation, and the more difficult it is to form stable hydration product nuclei in the RAC system. This is consistent with the result in Table 6, where the crystallization nucleation index n decreases with the increase of R_{aw}. The duration of the I process gradually shortens with the increase of R_{aw}. When $D_{im} + R_{aw} = 1.0$, the three curves characterizing the NG, I, and D reaction processes intersect at one point, indicating that the hydration reaction of RAC does not go through the I process. This is due to the excessive mixing water added to this group of RAC samples, resulting in a very high degree of ion undersaturation in the solution, allowing cement to rapidly hydrate and form $Ca(OH)_2$. Additionally, the other role of the additional water is to provide more space for the crystal growth of hydration products. Therefore, the hydration reaction directly transitions from the NG process to the D process.

Table 6
Hydration kinetic parameters.

No.	n	$p_{NG}n$	K_{NG}	K_I	K_D
RAC0 + 0	1.05624	1.80	0.04391	0.00594	0.00115
RAC0 + 0.6	1.08884	1.70	0.03295	0.00300	0.00108
RAC0 + 0.7	1.11539	1.65	0.03133	0.00262	0.00106
RAC0 + 0.8	1.08984	1.66	0.02983	0.00241	0.00102
RAC0 + 0.9	1.11765	1.65	0.02919	0.00219	0.00097
RAC0 + 1.0	1.11643	1.61	0.02908	0.00204	0.00091
RAC0.25 + 0	1.11864	1.53	0.03910	0.00417	0.00111
RAC0.25 + 0.35	1.10196	1.50	0.03404	0.00308	0.00106
RAC0.25 + 0.45	1.12868	1.43	0.03332	0.00284	0.00101
RAC0.25 + 0.55	1.15171	1.41	0.03206	0.00237	0.00095
RAC0.25 + 0.65	1.15857	1.40	0.03152	0.00225	0.00094
RAC0.25 + 0.75	1.17252	1.39	0.03199	0.00211	0.00091
RAC0.5 + 0	1.16923	1.38	0.03611	0.00313	0.00100
RAC0.5 + 0.1	1.17750	1.38	0.03685	0.00343	0.00104
RAC0.5 + 0.2	1.19265	1.35	0.03429	0.00269	0.00098
RAC0.5 + 0.3	1.18957	1.35	0.03280	0.00235	0.00092
RAC0.5 + 0.4	1.17313	1.35	0.03183	0.00212	0.00089
RAC0.5 + 0.5	1.18165	1.35	0.03177	0.00199	0.00088
RAC0.75 + 0	1.11277	1.44	0.03556	0.00339	0.00096
RAC0.75 + 0.05	1.11864	1.46	0.03644	0.00279	0.00094
RAC0.75 + 0.15	1.10058	1.44	0.03289	0.00238	0.00091
RAC0.75 + 0.25	1.12530	1.42	0.03252	0.00220	0.00087
RAC1.0 + 0	1.13944	1.38	0.03557	0.00269	0.00091

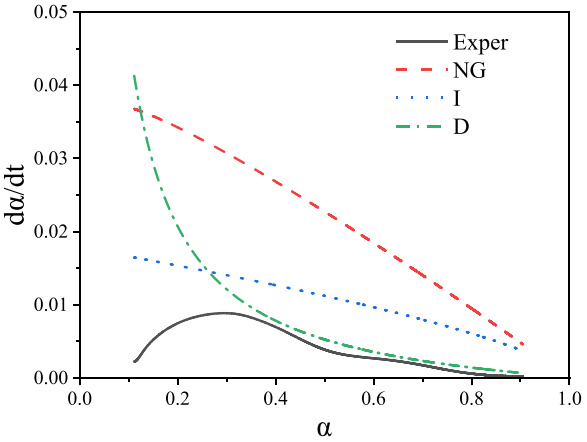

Fig. 9. Krstulovic-Dabic model fitting before modification.

Table 7
Correction factors (p_i and q_i).

Process	Formula	Correlation	Standard deviation
NG	$p_{NG} = 1.55295 – 0.47323D_{im} – 0.18415R_{aw}$	0.71	0.50
	$q_{NG} = -0.0223 + 0.00557D_{im} + 0.00821R_{aw}$	0.90	0.81
I	$p_I = 0.58158 + 0.63037D_{im} + 0.66673R_{aw}$	0.92	0.85
	$q_I = 0$	-	-
D	$p_D = 0.77924 – 0.1786D_{im} – 0.2632R_{aw}$	0.85	0.73
	$q_D = -0.00032$	-	-

When $D_{im} = 0.25$, the hydration reaction rate curve of RAC is shown in Fig. 11. It can be found that the hydration reaction of RAC undergoes three processes of NG, I, and D when $D_{im} + R_{aw} = 0.9$. However, the hydration reaction of RAC undergoes only NG and D processes when $D_{im} + R_{aw} = 1.0$. The corrected crystallization nucleation index $p_{NG}n$ gradually decreases with the increase of R_{aw}, as shown in Table 6. These patterns are the same as those of the RAC samples in the $D_{im} = 0$ series.

When the D_{im} value increases to 0.5, the water absorption rate and capacity of RA are significantly reduced. At the same time, the amount of additional water in this series of RAC mixtures can be maintained at a higher level (relative to when D_{im}=0.75, 1.0). These

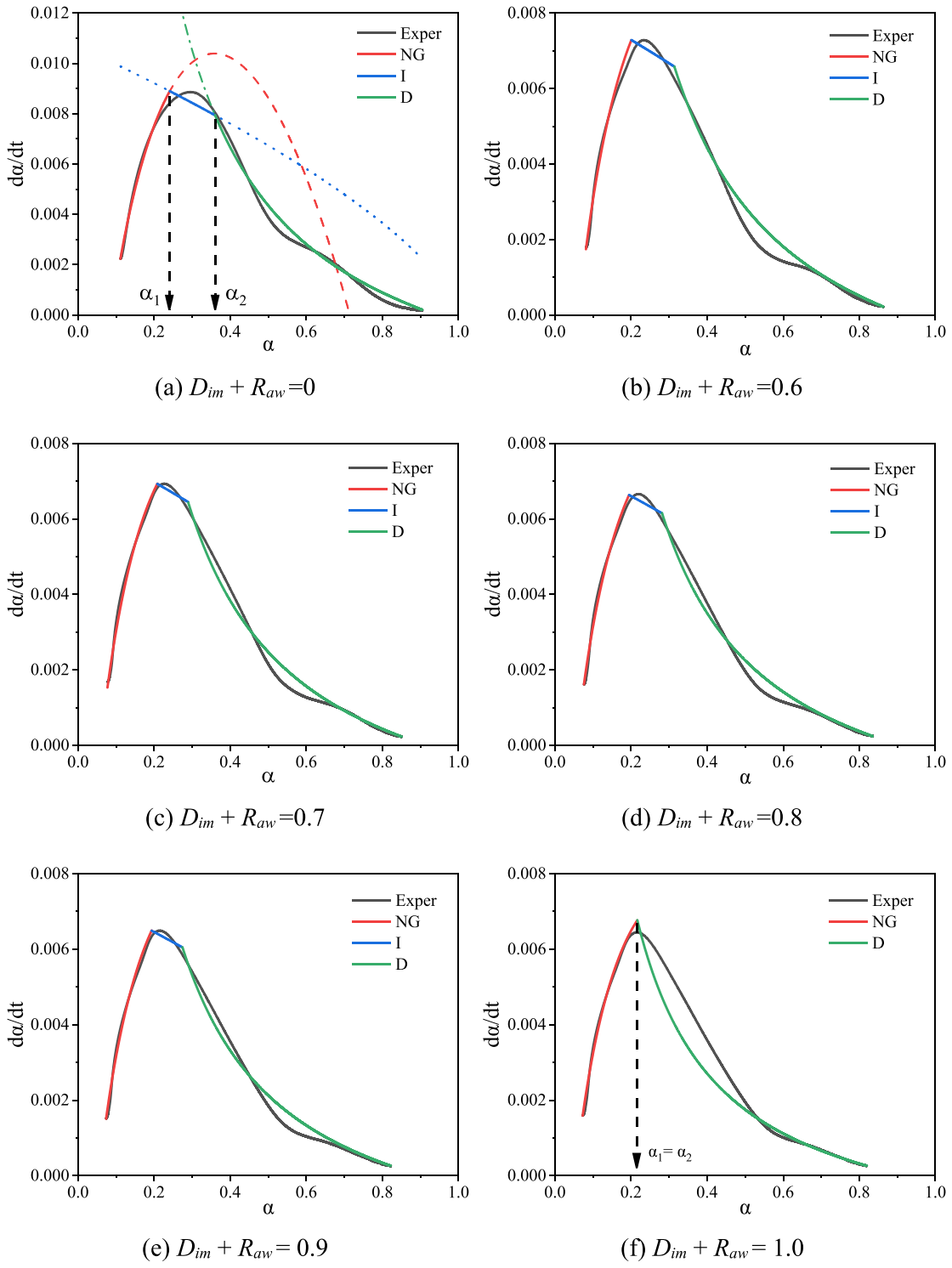

Fig. 10. Simulated hydration curves of RAC with D_{im}= 0 RA.

two reasons lead to the hydration characteristics of this series of RAC samples being different from those of other series. Data from Table 6 indicates that when $D_{im} \geq 0.5$, the crystallization nucleation index $p_{NG}n$ hardly changes with the increase of R_{aw}, but stabilizes at a certain level. As shown in Fig. 12(a-c), when $D_{im} = 0.5$ and $D_{im} + R_{aw} \leq 0.7$, the RAC hydration reaction undergoes three processes of NG, I, and D. When $D_{im} + R_{aw} > 0.7$, the RAC hydration reaction undergoes two processes of NG and D.

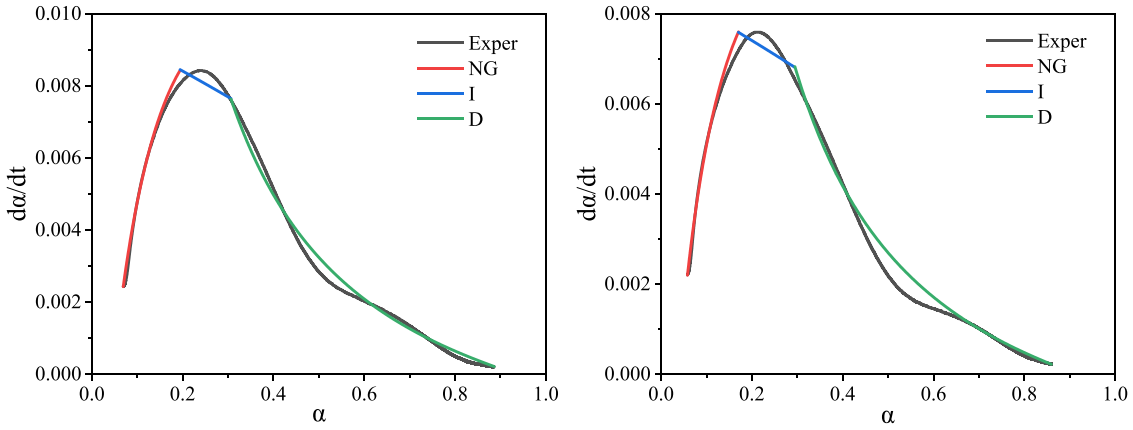

(a) $D_{im} + R_{aw} = 0.25$

(b) $D_{im} + R_{aw} = 0.6$

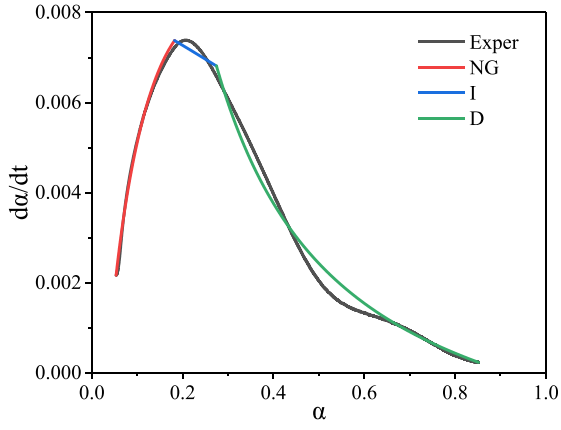

(c) $D_{im} + R_{aw} = 0.7$

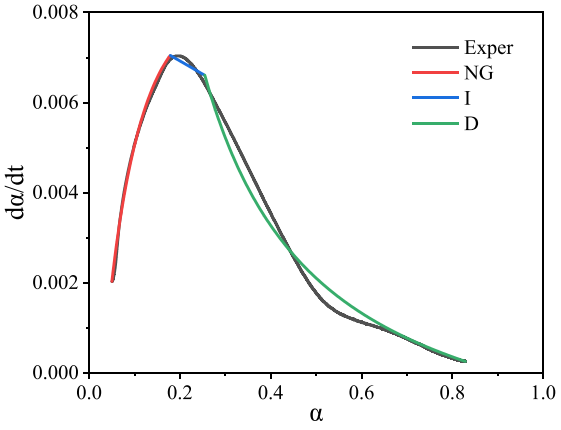

(d) $D_{im} + R_{aw} = 0.8$

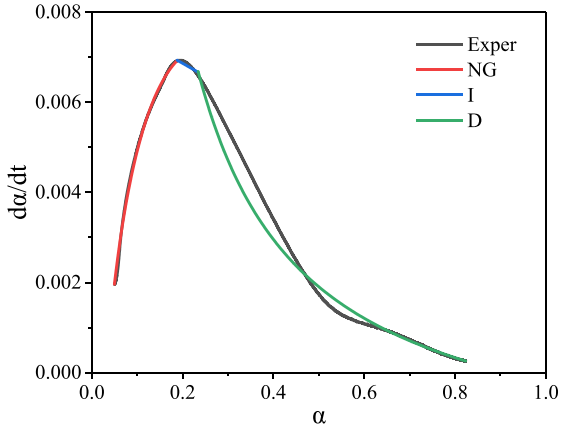

(e) $D_{im} + R_{aw} = 0.9$

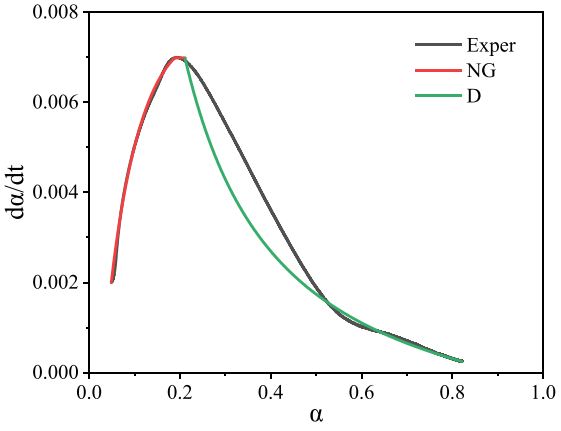

(f) $D_{im} + R_{aw} = 1.0$

Fig. 11. Simulated hydration curves of RAC containing D_{im}= 0.25 RA.

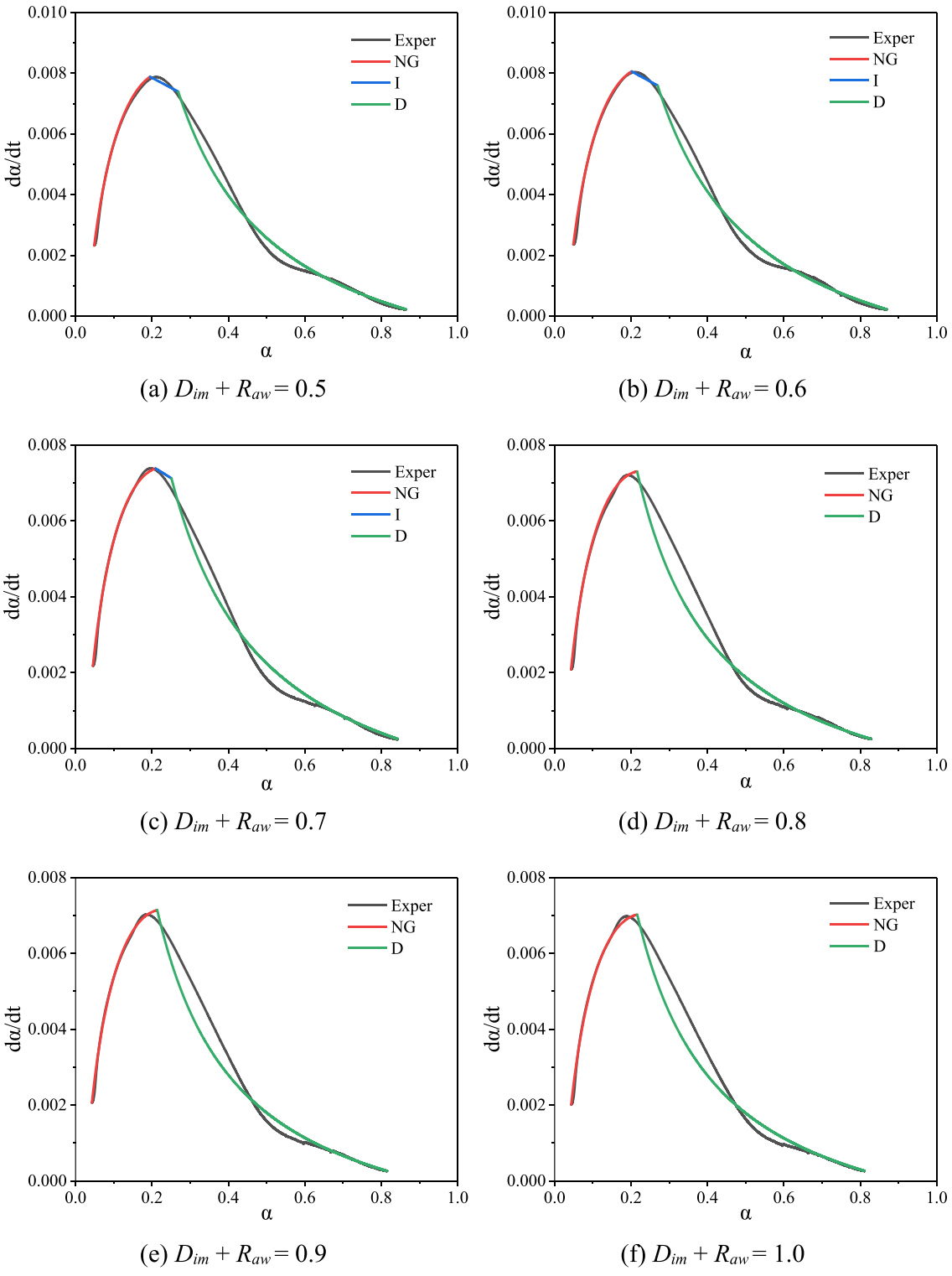

Fig. 12. Simulated hydration curves of RAC containing D_{im}= 0.5 RA.

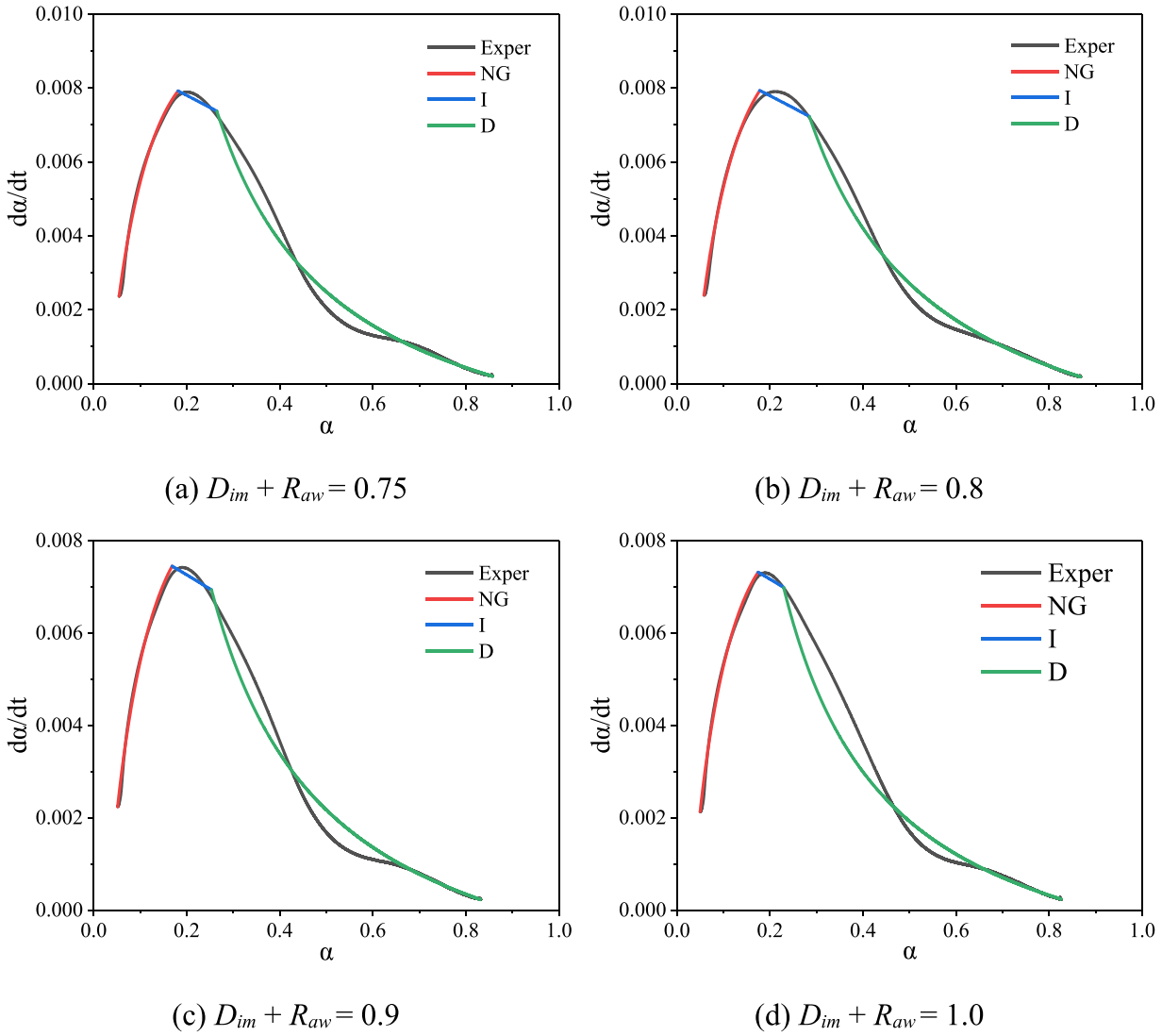

Fig. 13. Simulated hydration curves of RAC containing D_{im}= 0.75 RA.

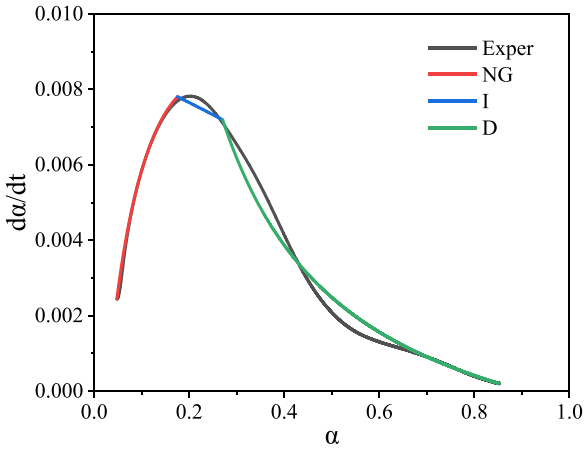

Fig. 14. Simulated hydration curves of RAC containing D_{im}= 1.0 RA.

Table 8
Hydration process of RAC.

No.	Hydration process	α_1	α_2	α_1-α_2
RAC0 + 0	NG-I-D	0.24115	0.36029	0.11914
RAC0 + 0.6	NG-I-D	0.20095	0.31400	0.11305
RAC0 + 0.7	NG-I-D	0.20813	0.28945	0.08132
RAC0 + 0.8	NG-I-D	0.19481	0.28146	0.08665
RAC0 + 0.9	NG-I-D	0.19395	0.27550	0.08155
RAC0 + 1.0	NG-D	0.21656		-
RAC0.25 + 0	NG-I-D	0.19449	0.30526	0.11077
RAC0.25 + 0.35	NG-I-D	0.17050	0.29482	0.12432
RAC0.25 + 0.45	NG-I-D	0.18234	0.27454	0.0922
RAC0.25 + 0.55	NG-I-D	0.17909	0.25486	0.07577
RAC0.25 + 0.65	NG-I-D	0.18894	0.23329	0.04435
RAC0.25 + 0.75	NG-D	0.20768		-
RAC0.5 + 0	NG-I-D	0.19495	0.26877	0.07382
RAC0.5 + 0.1	NG-I-D	0.20160	0.26979	0.06819
RAC0.5 + 0.2	NG-I-D	0.20956	0.25100	0.04144
RAC0.5 + 0.3	NG-D	0.21605		-
RAC0.5 + 0.4	NG-D	0.21401		-
RAC0.5 + 0.5	NG-D	0.21634		-
RAC0.75 + 0	NG-I-D	0.18134	0.26493	0.08395
RAC0.75 + 0.05	NG-I-D	0.17784	0.28475	0.10691
RAC0.75 + 0.15	NG-I-D	0.16856	0.25318	0.08462
RAC0.75 + 0.25	NG-I-D	0.17434	0.25016	0.07582
RAC1.0 + 0	NG-I-D	0.17526	0.27038	0.09512

When $D_{im}\geq$ 0.75 for RA, the water absorption rate and capacity of RA decrease to very low levels. At the same time, the amount of additional water in the RAC mixture is maintained at a lower level. These two factors can lead to a relatively high concentration of ionic solutions in the early paste. The transition between the three processes of the hydration reaction is relatively smooth and the I process reappears. The RAC hydration reaction goes through all three processes of NG, I, and D, as shown in Figs. 13 and 14.

3.5. Degree of hydration (DoH)

The influence of D_{im} and R_{aw} on the DoH $\alpha(t)$ of RAC calculated by Eq. 12 is shown in Figs. 15 and 16. As indicated in Eq. 12, $\alpha(t)$ is the ratio of the cumulative heat of hydration $Q(t)$ over time t to the total heat of hydration Q_{max} at the end of the hydration reaction. Therefore, it is necessary to comprehensively analyze the development law of RAC hydration degree by combining $\alpha(t)$ and Q_{max} data in Table 5.

As shown in Fig. 15(a), the smaller the D_{im} value of RA, the higher the DoH of RAC. When $D_{im}\leq$ 0.25, the growth rate decreases significantly after 60 h, and the DoH enters a slow rise phase. When $D_{im}\geq$ 0.5, although the DoH is relatively low, the rate of decrease also relatively slow. The DoH of RAC does not enter a slow rise phase until after 96 h. As depicted in Fig. 15(b), the DoH of RAC at the age of 7 days $\alpha(7d)$ decreases with the increase of D_{im}. This is due to the fact that the smaller the D_{im} value of RA, the less water is stored internally. On the one hand, more water will be absorbed by the RA from the slurry in the early stage of hydration. On the other hand,

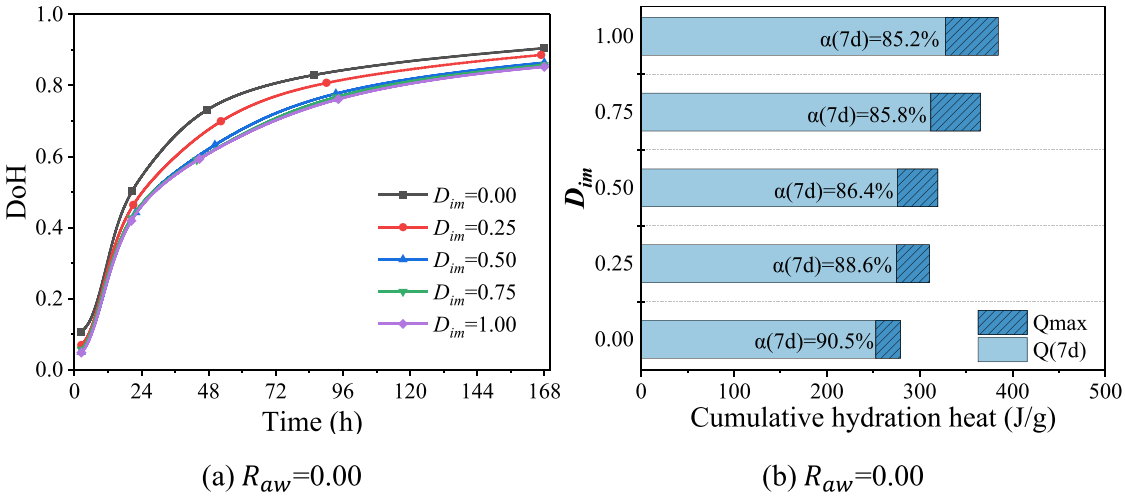

Fig. 15. Effect of D_{im} on DoH of RAC.

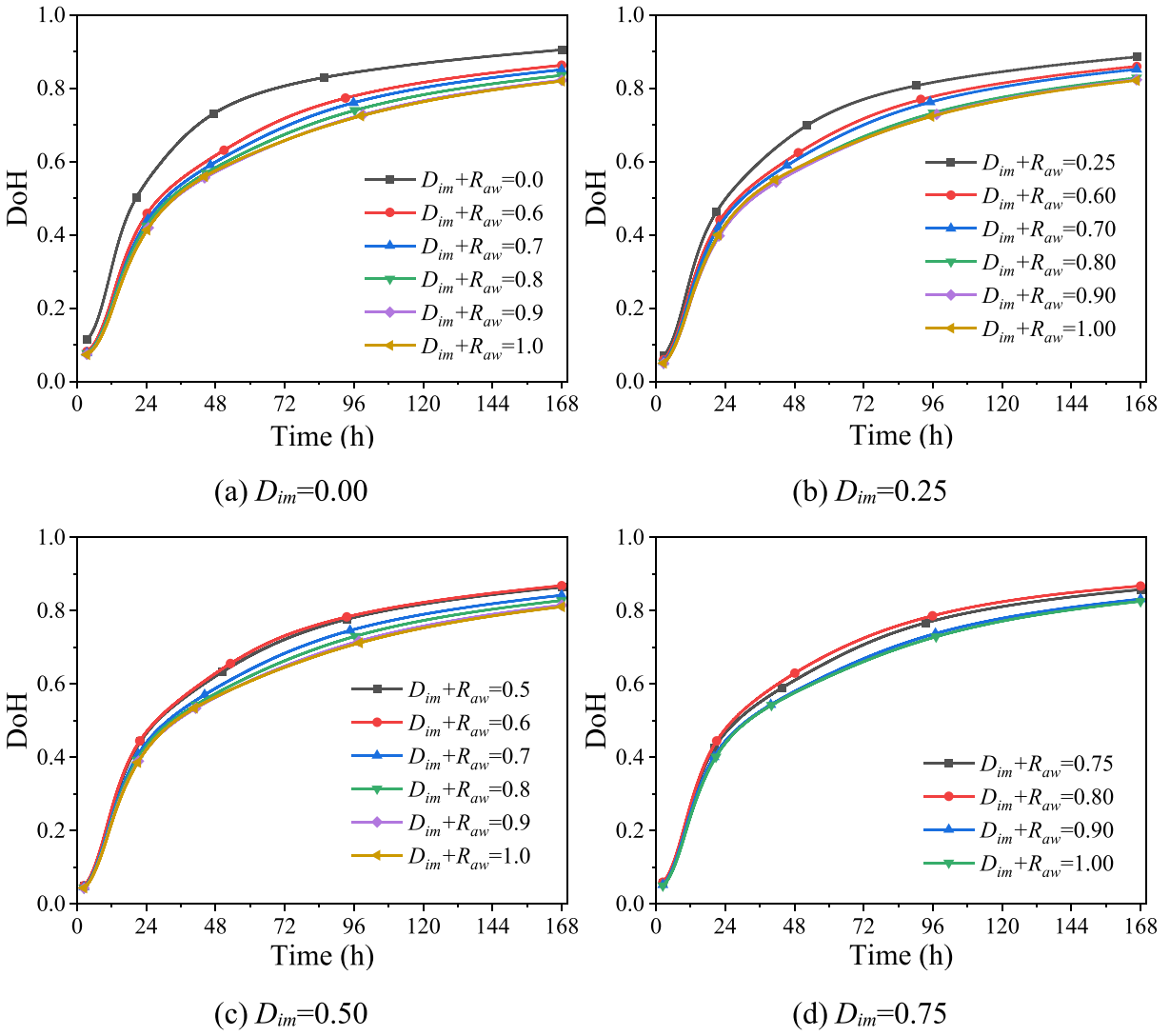

Fig. 16. Effect of R_{aw} on DoH of RAC.

less water will be released from these RA into the slurry in the later stages of hydration. RA with the low D_{im} values significantly reduce the total heat of hydration Q_{max}, but enhance the DoH of the RAC. However, this means that there is less space for subsequent hydration of RAC. In summary, RA with low D_{im} values essentially limits the hydration of RAC.

The influence of R_{aw} on the DoH of RAC is shown in Fig. 16. When D_{im} is fixed at a certain level, the DoH of RAC decreases with the increase of R_{aw} value. Combining the data in Table 5 with Fig. 6, the cumulative heat release $Q(t)$ and total heat release Q_{max} of RAC both increase significantly with the increase of R_{aw} value. Compared with the RAC specimens without additional mixing water (i.e., R_{aw}=0), additional water to RA saturation can increase $Q(7d)$ and Q_{max} of RAC by 9.3 %–42.8 % and 6.8 %–57.7 %, respectively. This indicates that additional water can not only effectively promote the early hydration reaction of RAC, but also enhance the later hydration potential. Moreover, for RAC specimens with lower D_{im} values, the positive effect of additional water on hydration is more obvious. When the D_{im} value is higher, the promotion effect of additional water on RAC hydration is weakened. In this case, the amount of additional water can be appropriately reduced at the design stage of the RAC proportion.

The above analyzes the regularity of the effects of D_{im} and R_{aw} on the degree of RAC hydration, respectively. In addition, when the effect of D_{im} + R_{aw} on the DoH of RAC is analyzed comprehensively, the results also show a strong regularity. As shown in Fig. 17, when the sum of D_{im} and R_{aw} is the same, the development law of degree of RAC hydration over time is almost identical. However, combining the data analysis from Table 5, the smaller the sum of D_{im} + R_{aw}, the more concentrated the values of Q_{max} and $Q(7d)$ for RAC samples. As the value of D_{im} + R_{aw} increases, the values of Q_{max} and $Q(7d)$ for RAC from different experimental groups gradually diverge. This indicates that when the D_{im} of RA is different, it is entirely possible to adjust the amount of additional water to achieve the same DoH of RAC at the same time.

However, for RAC samples with the same value of D_{im} + R_{aw}, the differences in cumulative heat of hydration $Q(t)$ due to the

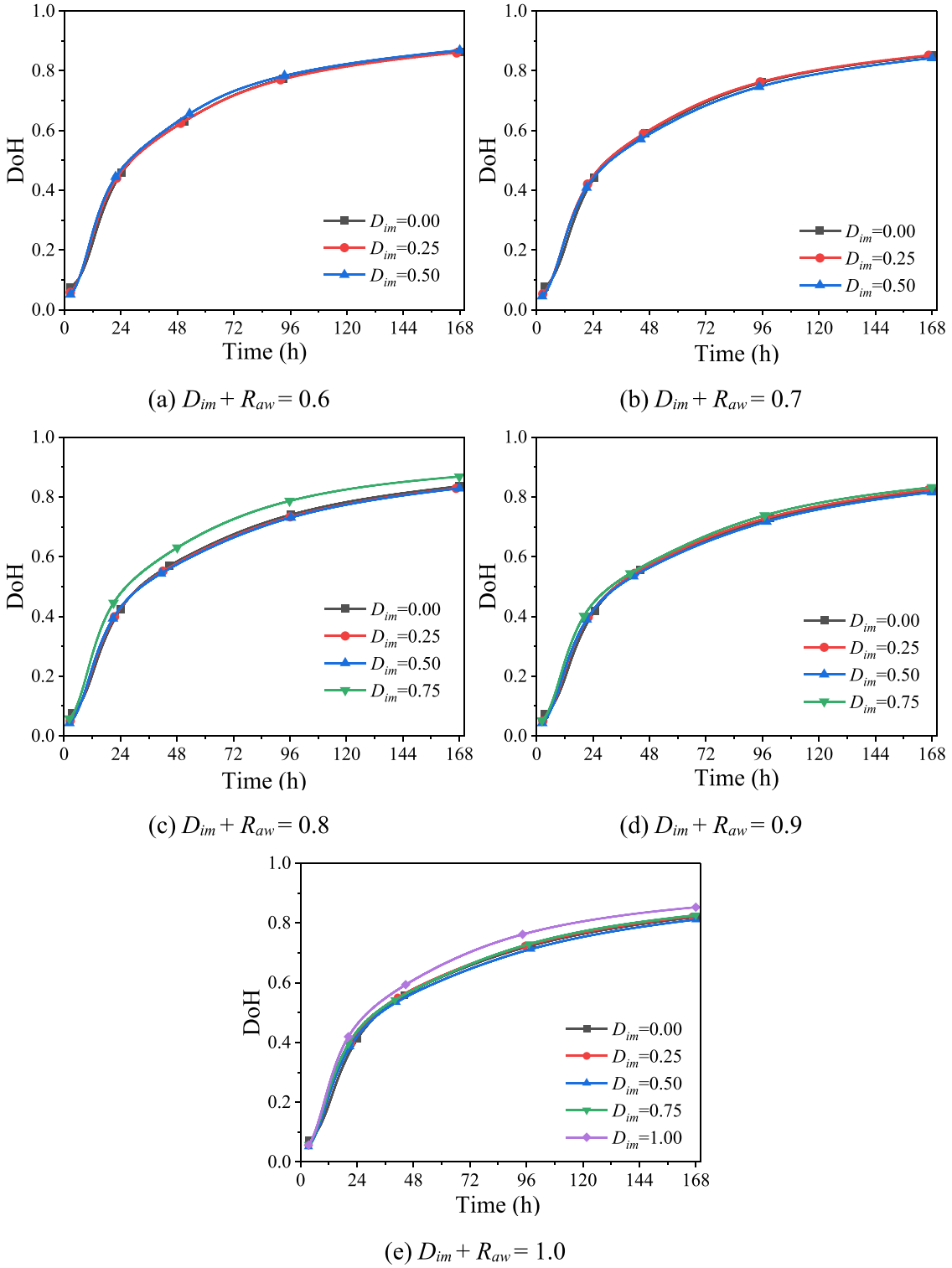

Fig. 17. DoH of RAC with constant $D_{im} + R_{aw}$ and varied D_{im} and R_{aw}.

differences in D_{im} and R_{aw} should not be overlooked. This can lead to differences in the performance of RAC.

3.6. Effective water to cement ratio

The RC samples were prepared according to the mix ratio shown in Table 4 and the cumulative hydration heat release curves were measured. The w/c ratio of the RC samples gradually increased from 0.34 to 0.64 with a gradient of 0.02. Typically, when preparing RC samples with natural sand, the water absorption behavior of the aggregate is not considered. Furthermore, the water absorption rate of the ISO standard sand used in this study is only 0.9 %, which can be completely neglected. Therefore, the nominal w/c ratio of the RAC can be considered as the effective w/c ratio. The total hydration heat release Q_{max} values of RC samples can be obtained by substituting the test data of isothermal calorimetry into Eq. 11. The results show that there is a one-to-one correspondence between Q_{max} and the effective w/c ratio. The quantitative relationship between Q_{max} and the effective w/c ratio was established, as shown in Fig. 18. Then, the effective w/c ratio of RAC can be obtained by substituting the Q_{max} values of the RAC specimens in Table 5 into the function in Fig. 18.

In order to comprehensively analyze the effect of water absorption and release behavior of RA in slurry on the w/c ratio, this paper compares the nominal w/c ratio, the effective w/c ratio, and the upper and lower limits of w/c ratio of RAC. The nominal w/c ratio is the ratio of the mass of mixing water to the mass of cement used in the preparation of RAC specimens, as shown in Table 5. The effective w/c ratio is calculated by substituting the Q_{max} value of RAC obtained according to the kinetic theory of hydration kinetics into the function shown in Fig. 18. The upper limit value of the w/c ratio corresponds to the extreme case when all the water inside the RAs is released into the slurry. The lower limit value of the w/c ratio corresponds to the extreme case when RAs absorb water from the paste and reaches saturation.

The D_{im} value of RA has a significant impact on the effective w/c ratio of RAC, as shown in Fig. 19. When $D_{im} \leq 0.5$, RA primarily exhibits water-absorbing characteristics. The direction of water transport within the RAC system is from the paste to the RA. This leads to the effective w/c ratio that is lower than the nominal w/c ratio in the mix design. When $D_{im} \geq 0.75$, RA primarily exhibits water-releasing characteristics. The direction of water transport within the RAC system is from the RA to the paste. This results in the effective w/c ratio of RAC is greater than the nominal w/c ratio. Furthermore, a functional relationship between the effective w/c ratio of RAC and the D_{im} value of RA has been established, as shown in Fig. 19. The critical value of D_{im} at which the effective w/c ratio equals the nominal w/c ratio is 0.65. When this condition is met, the water transport between RA and the paste reaches equilibrium.

The influence of R_{aw} value on the effective w/c ratio is shown in Fig. 20. When the D_{im} value remains constant, the effective w/c ratio of RAC gradually increases with the increase of R_{aw} value. When $D_{im} \leq 0.5$, the water absorption behavior of RA causes the effective w/c ratio to be less than the nominal w/c ratio, as seen in Fig. 20(a)(b)(c). When $D_{im} \geq 0.75$, the water released from RA into the paste causes the effective w/c ratio to be greater than the nominal w/c ratio, as seen in Figs. 20(d) and 21(e). This phenomenon is basically consistent with the result mentioned earlier that RA with $D_{im} = 0.65$ can achieve a balance in water transport with the paste. The higher the D_{im} value of RA, the smaller the increase and the rate of increase of the effective w/c ratio with R_{aw}. Eventually, the slope of the effective w/c ratio curve is close to that of the nominal w/c ratio curve. This indicates that when R_{aw} increases to a certain extent, it essentially satisfies the water absorption of RA. Beyond this critical value, the additional water, not absorbed by the aggregate, remains in the paste.

When the sum of D_{im} and R_{aw} remains constant but D_{im} and R_{aw} vary separately, the development law of the effective w/c ratio is shown in Fig. 21. With a fixed sum of D_{im} and R_{aw}, a larger D_{im} implies a smaller R_{aw}. Although RA with a larger D_{im} value has a slower water absorption rate, it starts from a higher absorption point. Therefore, for RAC samples with a larger D_{im} and a smaller R_{aw}, there is less water in the paste and the w/c ratio is also smaller. Therefore, when the sum of D_{im} and R_{aw} remains constant, the effective w/c ratio of RAC decreases with the increase of D_{im} (and the decrease of R_{aw}). When $D_{im} + R_{aw} \leq 0.7$, the effective w/c ratio of RAC is less than the nominal w/c ratio. When $D_{im} + R_{aw} \geq 0.8$, the rate of decrease of the effective w/c ratio is slower than that of the nominal w/c

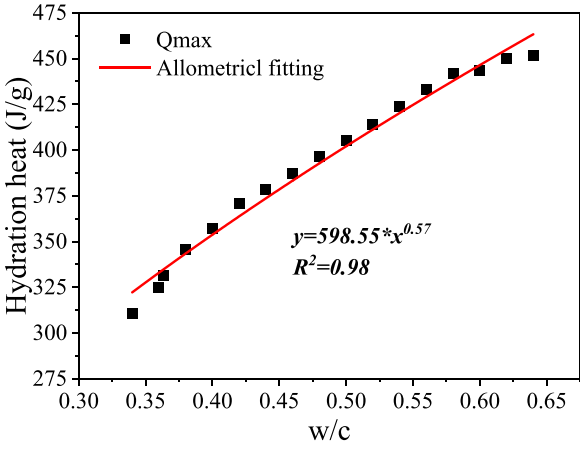

Fig. 18. W/C ratio index fitting of RC.

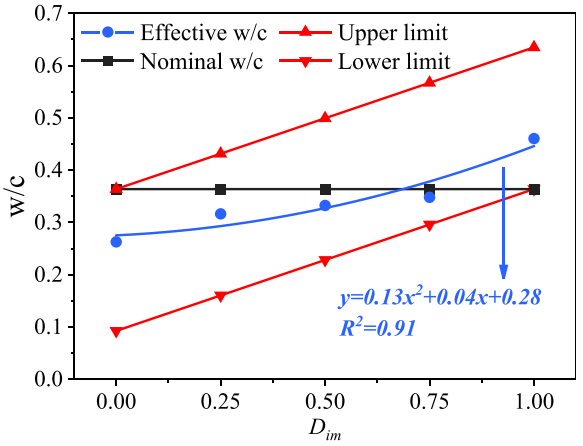

Fig. 19. Effect of D_{im} value on the effective w/c ratio.

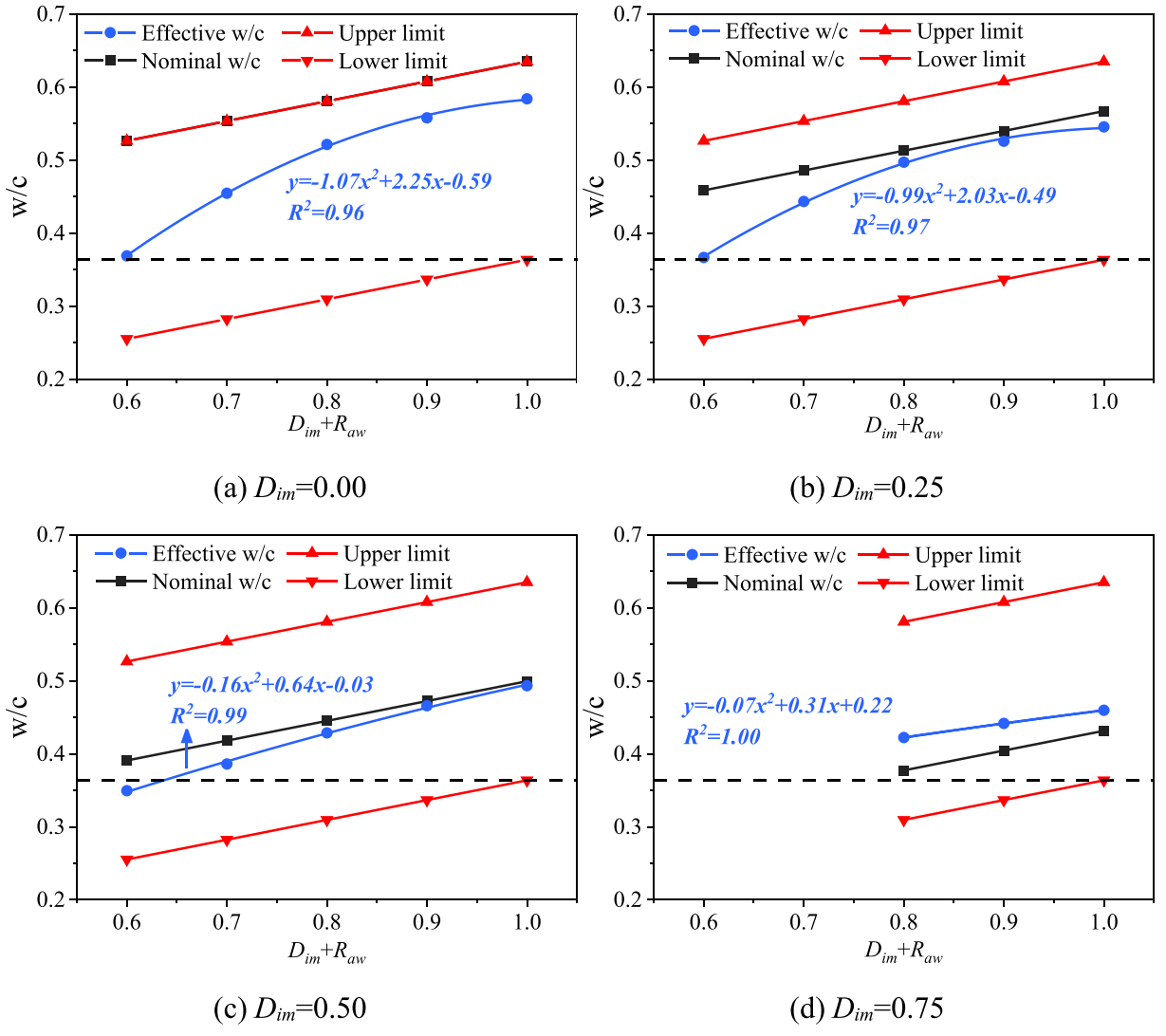

Fig. 20. Effect of R_{aw} value on the effective w/c ratio.

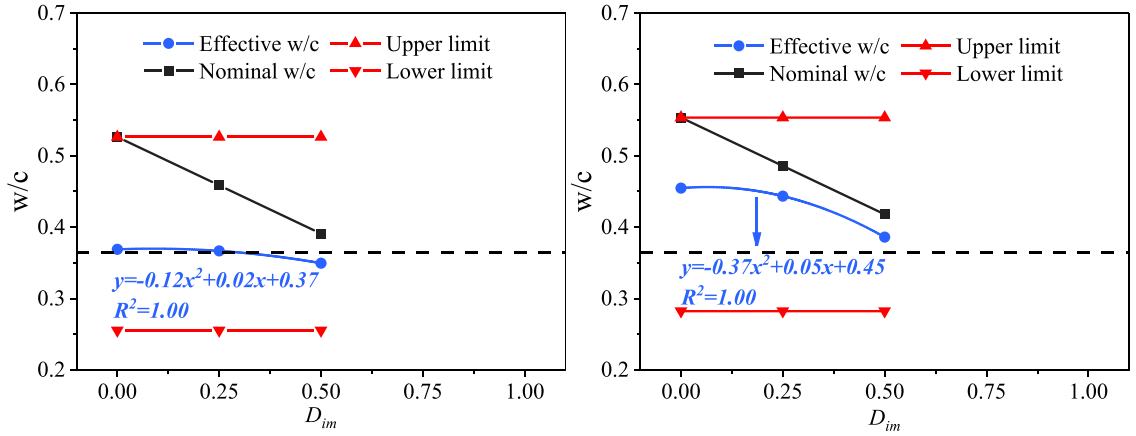

(a) $D_{im} + R_{aw} = 0.6$

(b) $D_{im} + R_{aw} = 0.7$

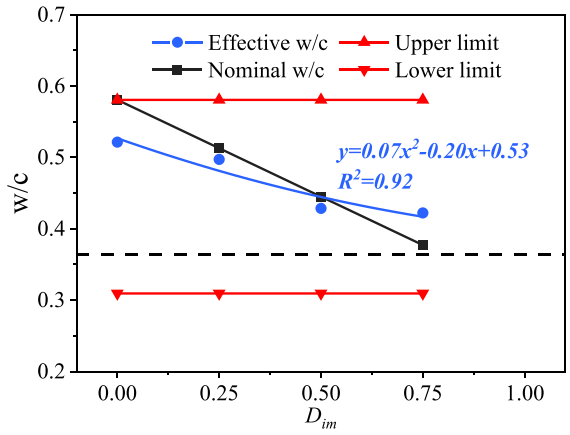

(c) $D_{im} + R_{aw} = 0.8$

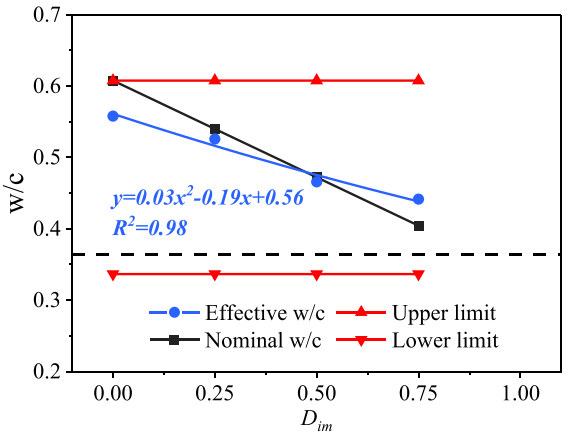

(d) $D_{im} + R_{aw} = 0.9$

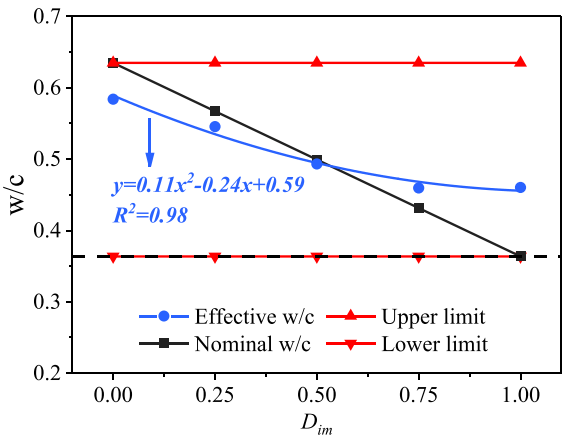

(e) $D_{im} + R_{aw} = 1.0$

Fig. 21. Effective w/c ratio of RAC.

ratio. Additionally, there is an intersection point between the curves of the effective w/c ratio and the nominal w/c ratio. Before the intersection point, RA mainly exhibits water absorption. After the intersection point, RA mainly exhibits water release.

4. Conclusions

Previous studies have focused on quantifying RA water absorption or correlating w/c ratios with RAC properties but lacked insights into how RA moisture dynamics influence hydration kinetics. This research investigated the effects of RA initial moisture degree (D_{im}) and additional water ratio (R_{aw}) on RAC hydration behavior. A modified Krstulovic-Dabic hydration kinetics model was developed to account for RA water absorption and release, enabling precise analysis of hydration mechanisms. Key findings include:

(1) RA with low D_{im} (≤ 0.5) absorbed water from the paste, reducing cumulative hydration heat by up to 11.8 % compared to reference. Conversely, RA with high D_{im} (≥ 0.75) released stored water, enhancing hydration heat by up to 14.3 % through internal curing. The induction period of hydration shortened with increasing D_{im}, while R_{aw} prolonged the deceleration phase, mitigating declines in hydration rate.
(2) Two correction coefficients correlated with D_{im} and R_{aw} were introduced to improve the Krstulovic-Dabic model's accuracy for RAC. The modified model effectively captured hydration stages of nucleation and crystal growth, interactions at phase boundaries, and diffusion. It revealed that (i) the duration of the interactions at phase boundaries process gradually shortens and even disappears with the increase of R_{aw} under low D_{im} (≤ 0.5); and (ii) higher D_{im} or R_{aw} increased total hydration heat and extended hydration potential.
(3) A critical D_{im} threshold of 0.65 was identified, where water transport equilibrium between RA and paste ensures the effective w/c ratio equals the nominal value. For $D_{im} \leq 0.5$, effective w/c ratios fell below nominal values due to RA water absorption; for $D_{im} \geq 0.75$, effective w/c ratios exceeded nominal values as RA released water. Adjusting R_{aw} allowed precise control of effective w/c ratios, with higher R_{aw} amplifying hydration promotion in low-D_{im} RAC.
(4) By coupling the D_{im}–R_{aw} framework with on-site moisture metering, practitioners can pre-calculate and lock the effective w/c ratio prior to batching, eliminating the empirical loops traditionally used to balance workability, strength and durability; a single verification pour is then sufficient to translate the laboratory protocol into a robust, site-ready control procedure.

In light of the methodological gaps identified in existing literature, this work recommends that future investigations prioritize the quantification of the effects of D_{im} of RA and R_{aw} on the mechanical properties, long-term properties and durability of the concrete of RAC. Also, it is suggested that predict the properties by using the method proposed in this paper and evaluate effect of moisture transfer on microstructure and properties of ITZ between new and old mortar and between new mortar and original aggregate. This is of great significance for improving the quality of RA and RAC performance.

CRediT authorship contribution statement

Tianyong Huang: Writing – review & editing, Validation, Conceptualization. **ZOU Shuai:** Writing – review & editing, Validation, Methodology, Conceptualization. **Julun Li:** Writing – original draft, Methodology, Investigation, Data curation, Conceptualization. **Zhenhua Duan:** Writing – review & editing, Validation, Supervision, Methodology, Funding acquisition, Conceptualization. **Long Li:** Writing – review & editing, Methodology, Conceptualization. **Zhangli Hu:** Writing – review & editing, Validation, Methodology, Conceptualization. **Bo Li:** Writing – review & editing, Methodology, Conceptualization.

Declaration of Competing Interest

The authors declare that they have no known competing financial interests or personal relationships that could have appeared to influence the work reported in this paper.

Acknowledgements

The financial support from National Natural Science Foundation of China (No. 52178244), and laboratory equipment support from Beijing NELD Intelligent Technology Co., Ltd.

Data availability

Data will be made available on request.

References

[1] Y. Zhang, S. Hu, F. Guo, et al., Assessing the potential of decarbonizing China's building construction by 2060 and synergy with industry sector, J. Clean. Prod. 359 (2022) 132086.
[2] J.Z. Xiao, S. Zou, C.S. Poon, et al., We use 30 billion tonnes of concrete each year — here's how to make it sustainable, Nature 638 (2025) 888–890.
[3] C.F. Dunant, S. Joseph, R. Prajapati, et al., Electric recycling of portland cement at scale, Nature 629 (2024) 1055–1061.

[4] B. Chen, Y. Zhao, L. Peng, Long-term performance of recycled aggregate concrete beams exposed to 10 years of loading and chloride environments, Eng. Struct. 333 (2025).
[5] E. Kravchenko, G. Lazorenko, X. Jiang, et al., Alkali-activated materials made of construction and demolition waste as precursors: a review, Sustain. Mater. Techno 39 (2024).
[6] L.A.L. Ruiz, X.R. Ramon, S.G. Domingo, The circular economy in the construction and demolition waste sector - a review and an integrative model approach, J. Clean. Prod. 248 (2020) 119238.
[7] J.Z. Xiao, S. Zou, Cement at 200: towards net-zero fully recycled concrete, Nature 631 (2024), 740-740.
[8] J.Z. Xiao, H.H. Zhang, Y.X. Tang, et al., Fully utilizing carbonated recycled aggregates in concrete: strength, drying shrinkage and carbon emissions analysis, J. Clean. Prod. 377 (2022).
[9] J. Kim, Influence of quality of recycled aggregates on the mechanical properties of recycled aggregate concretes: an overview, Constr. Build. Mater. 328 (2022).
[10] Z.H. Duan, C.S. Poon, Properties of recycled aggregate concrete made with recycled aggregates with different amounts of old adhered mortars, Mater. Des. 58 (2014) 19–29.
[11] X.G. Chen, Z. Sierens, E. Gruyaert, et al., Precast concrete wall panels incorporating mixed recycled aggregates, Acids Mater. J. 120 (2023) 75–88.
[12] B. Wang, L.B. Yan, Q.N. Fu, et al., A comprehensive review on recycled aggregate and recycled aggregate concrete, Res. Cons. Recy 171 (2021) 105565.
[13] D. Peiris, C. Gunasekara, D.W. Law, et al., Impact of treatment methods on recycled concrete aggregate performance: a comprehensive review, Environ. Sci. Pollut. Res. 32 (2025) 14405–14438.
[14] K.C. Onyelowe, V. Kamchoom, S. Hanandeh, et al., Physics-informed modeling of splitting tensile strength of recycled aggregate concrete using advanced machine learning, Sci. Rep. 15 (2025) 7135.
[15] H. Maedeh, D. Mehdi, S. Hojjat, A comprehensive quantitative bottom-up analysis of fiber-reinforced recycled-aggregate concrete behavior, Sci. Rep. 13 (2023) 4502.
[16] A.Z. Bendimerad, E. Roziere, A. Loukili, Combined experimental methods to assess absorption rate of natural and recycled aggregates, Mater. Struct. 48 (2015) 3557–3569.
[17] M. Quattrone, B. Cazacliu, S.C. Angulo, et al., Measuring the water absorption of recycled aggregates, what is the best practice for concrete production? Constr. Build. Mater. 123 (2016) 690–703.
[18] M.E. Sosa, L.E. Carrizo, C.J. Zega, et al., Water absorption of fine recycled aggregates: effective determination by a method based on electrical conductivity, Mater. Struct. 51 (2018) 127.
[19] V.W.Y. Tam, X.G. Gao, C.M. Tam, et al., New approach in measuring water absorption of recycled aggregates, Constr. Build. Mater. 22 (2008) 364–369.
[20] A.D. Tegguer, Determining the water absorption of recycled aggregates utilizing hydrostatic weighing approach, Constr. Build. Mater. 27 (2012) 112–116.
[21] Z.H. Duan, W.J. Zhao, T.H. Ye, et al., Measurement of water absorption of recycled aggregate, Mater 15 (2022) 5141.
[22] Y.H. Wu, Z.D. Qi, M.D. Niu, et al., Effect of moisture condition of brick-concrete recycled coarse aggregate on the properties of concrete, Mater 15 (2022) 7204.
[23] S.M. Andres, C.W. Chung, B.E.M. Rada, Interaction effect of recycled aggregate type, moisture state, and mixing process on the properties of high-performance concretes, Case Stud. Constr. Mater. 18 (2023) e02208.
[24] H.R. Zhang, X. Xu, W.S. Liu, et al., Influence of the moisture states of aggregate recycled from waste concrete on the performance of the prepared recycled aggregate concrete (RAC) – a review, Constr. Build. Mater. 326 (2022) 126891.
[25] H. Mefteh, Q. Kebaïli, H. Oucief, et al., Influence of moisture conditioning of recycled aggregates on the properties of fresh and hardened concrete, J. Clean. Prod. 54 (2013) 282–288.
[26] Y.X. Zhao, W.L. Zeng, H.R. Zhang, Properties of recycled aggregate concrete with different water control methods, Constr. Build. Mater. 152 (2017) 539–546.
[27] L. Ferreira, Jd Brito, M. Barra, Influence of the pre-saturation of recycled coarse concrete aggregates on concrete properties, Mag. Concr. Res. 63 (2011) 617–627.
[28] X.G. Chen, H.Y. Hao, Jd Brito, et al., Discussion of the implementation of water compensation methods for recycled aggregate concrete: a critical review, Cem. Concr. Compos. 161 (2025) 106080.
[29] C.F. Liang, H.L. Chen, R. Li, et al., Effect of additional water content and adding methods on the performance of recycled aggregate concrete, Constr. Build. Mater. 423 (2024) 135868.
[30] B.X. Li, P.B. Chen, S. Yin, et al., Effect of additional water amount on the workability and mechanical properties of concrete with recycled fine aggregates, Mater. Rev. 38 (2024).
[31] Z.F. Zhao, S. Remond, D. Damidot, et al., Influence of fine recycled concrete aggregates on the properties of mortars, Constr. Build. Mater. 81 (2015) 179–186.
[32] X.B. Zhang, Z. Fang, S.C. Deng, et al., Additional water use influencing strength and fluidity of recycled concrete, J. Cent. South Univ. Technol. 15 (2008) 221–224.
[33] Z.H. Duan, Q. Deng, J.Z. Xiao, et al., Early-stage water-absorbing behavior and mechanism of recycled coarse aggregate, Constr. Build. Mater. 394 (2023).
[34] Y.X. Tang, J.Z. Xiao, H.H. Zhang, et al., Mechanical properties and uniaxial compressive stress-strain behavior of fully recycled aggregate concrete, Constr. Build. Mater. 323 (2022).
[35] T. Li, R. Nogueira, Jd Brito, et al., A simple method to address the high water absorption of recycled aggregates in cementitious mixes, Constr. Build. Mater. 411 (2024) 134404.
[36] J.Z. Xiao, Y.X. Tang, H.H. Zhang, et al., Basic property and compressive damage constitutive model of full recycled aggregate concrete, J. Tongji Univ. Nat. Sci. 51 (2023) 1910–1918, 1982.
[37] J. Hu, Z. Ge, K.J. Wang, Influence of cement fineness and water-to-cement ratio on mortar early-age heat of hydration and set times, Constr. Build. Mater. 50 (2014) 657–663.
[38] S. Erdem, A.R. Dawson, N.H. Thom, Influence of the micro- and nanoscale local mechanical properties of the interfacial transition zone on impact behavior of concrete made with different aggregates, Cem. Concr. Res. 42 (2012) 447–458.
[39] A. Djerbi, Effect of recycled coarse aggregate on the new interfacial transition zone concrete, Constr. Build. Mater. 190 (2018) 1023–1033.
[40] K. Wu, H.S. Shi, L.L. Xu, et al., Microstructural characterization of ITZ in blended cement concretes and its relation to transport properties, Cem. Concr. Res. 79 (2016) 243–256.
[41] P. Devapura, T. Ginigaddara, D. Udumulla, et al., Effect of graphene oxide on interfacial transition zone and strength enhancement of recycled aggregate concrete, J. Build. Eng. 105 (2025) 112570.
[42] S.A. Memon, Z. Bekzhanova, A. Murzakarimova, A review of improvement of interfacial transition zone and adherent mortar in recycled concrete aggregate, Buildings 12 (2022).
[43] L. Xu, J.J. Wang, R. Huang, et al., Investigations on micro-mechanical properties of the ITZs between recycled aggregates and recycled cement paste, Constr. Build. Mater. 450 (2024).
[44] G. Xia, Y. Zhao, Interface parameters of recycled aggregate concrete considering the distribution of old mortar content, Case Stud. Constr. Mater. 20 (2024).
[45] I.F.S. del Bosque, W. Zhu, T. Howind, et al., Properties of interfacial transition zones (ITZs) in concrete containing recycled mixed aggregate, Cem. Concr. Compos. 81 (2017) 25–34.
[46] Y. Liu, P.F. Ren, N. Garcia-Troncoso, et al., Roles of enhanced ITZ in improving the mechanical properties of concrete prepared with different types of recycled aggregates, J. Build. Eng. 60 (2022).
[47] D.N. Qu, W.W. Lian, X.L. Fang, Characterization of the interfacial transition zone between wet carbonated fine recycled aggregate and fresh cement paste, Constr. Build. Mater. 458 (2025).
[48] J.Z. Xiao, W.G. Li, Z.H. Sun, et al., Properties of interfacial transition zones in recycled aggregate concrete tested by nanoindentation, Cem. Concr. Compos. 37 (2013) 276–292.
[49] M. Kim, S.H. Kang, S.G. Hong, et al., Influence of effective water-to-cement ratios on internal damage and salt scaling of concrete with superabsorbent polymer, Mater 12 (2019) 3863.

[50] M.E. Sosa, Y.A.V. Zaccardi, C.J. Zega, A critical review of the resulting effective water-to-cement ratio of fine recycled aggregate concrete, Constr. Build. Mater. 313 (2021) 125536.
[51] A. Paul, S. Murgadas, J. Delpiano, et al., The role of moisture transport mechanisms on the performance of lightweight aggregates in internal curing, Constr. Build. Mater. 268 (2021).
[52] Z. Li, J.P. Liu, J.Z. Xiao, et al., A method to determine water absorption of recycled fine aggregate in paste for design and quality control of fresh mortar, Constr. Build. Mater. 197 (2019) 30–41.
[53] P. Ge, W. Huang, H. Zhang, et al., Study on calculation model for compressive strength of water saturated recycled aggregate concrete, Ksce. J. Civ. Eng. 26 (2022) 273–285.
[54] J.T. Dang, R.F. Zhu, J.Z. Xiao, et al., Effect of surface activity of recycled fine aggregates from clay bricks on the hydration, microstructure and chloride transport of concrete, Constr. Build. Mater. 418 (2024) 135499.
[55] H. Maimouni, S. Remond, F. Huchet, et al., Quantitative assessment of the saturation degree of model fine recycled concrete aggregates immersed in a filler or cement paste, Constr. Build. Mater. 175 (2018) 496–507.
[56] A. Adessina, A.B. Fraj, J.F. Barthélémy, Improvement of the compressive strength of recycled aggregate concretes and relative effects on durability properties, Constr. Build. Mater. 384 (2023).
[57] D.P. Bentz, Influence of water-to-cement ratio on hydration kinetics: simple models based on spatial considerations, Cem. Concr. Res. 36 (2006) 238–244.
[58] G.T. Zhang, H.Y. Xia, H. Wang, et al., Early hydration characteristics and kinetics model of cement pastes containing internal curing materials with different absorption behaviors, Constr. Build. Mater. 383 (2023) 131412.
[59] Y. Abriak, D.C. Chu, W. Maherzi, et al., Influence of fine recycled concrete aggregates use on the hydration kinetics and mechanical–microstructural properties of hydrated cement: experimental and numerical approaches, Constr. Build. Mater. 408 (2023) 133769.
[60] F.H. Han, Z.Q. Zhang, J.H. Liu, et al., Effect of water-to-binder ratio on the hydration kinetics of composite binder containing slag or Fly ash, J. Therm. Anal. Calorim. 128 (2017) 855–865.
[61] GB/T 14684-2022, Sand for Construction [S], Beijing, 2022.
[62] GB/T 12959-2024, Test methods for heat of hydration of cement [S], Beijing, 2024.
[63] R. Krstulović, P. Dabić, A conceptual model of the cement hydration process, Cem. Concr. Res. 30 (2000) 693–698.
[64] G.D. Schutter, L. Taerwe, General hydration model for portland cement and blast furnace slag cement, Cem. Concr. Res. 25 (1995) 593–604.
[65] X. Sheng, S. Xiao, W. Zheng, et al., Hydration kinetics analysis of cementitious paste composites produced by binary and ternary binder materials for potential use in massive concrete structures, Case Stud. Constr. Mater. 18 (2023) e02209.
[66] X.Y. Wang, H.S. Lee, Modeling of hydration kinetics in cement based materials considering the effects of curing temperature and applied pressure, Constr. Build. Mater. 28 (2012) 1–13.
[67] Z.Q. Zhang, Y. Liu, L. Huang, et al., A new hydration kinetics model of composite cementitious materials, part 1: hydration kinetic model of portland cement, J. Am. Ceram. Soc. 103 (2020) 1970–1991.
[68] H. Zhao, G. Sun, L. Yu, et al., Hydration of early age cement paste with Nano-CaCO3 and SAP by LF NMR spectroscopy: mechanism and prediction, Model. Simul. Eng. 2019 (2019).
[69] P. Juilland, E. Gallucci, R. Flatt, et al., Dissolution theory applied to the induction period in alite hydration, Cem. Concr. Res. 40 (2010) 831–844.
[70] A.F.S. Gallardo, J.L. Provis, Early-age characterisation of portland cement by impedance spectroscopy, Adv. Cem. Res. 34 (2022) 542–559.
[71] Y.S. Zhao, J.M. Gao, G.F. Chen, et al., Early-age hydration characteristics and kinetics model of blended cement containing waste clay brick and slag, J. Build. Eng. 51 (2022) 104360.